SPAT-Horbury-2

Investigating the Solar Wind with Parker Solar Probe

Author:
Ronan Laker

Supervisor:
Prof. Timothy S. Horbury

Assessor:
Dr. Jonathan P. Eastwood

April, 2019

Imperial College
London

Abstract

Since the start of the space age, various spacecraft have supplied direct and remote observations of the solar wind. This has proved critical to our understanding of its structure and dynamics. However, there are still many unresolved questions, which provided the motivation behind the recently launched Parker Solar Probe (Probe); humanity's closest approach to the Sun. The aim of this study was to generate predictions of the solar wind conditions for the first perihelion pass, so that Probe's data could be better interpreted.

A large fluid dynamic simulation was first used to provide successful predictions of the solar wind velocity, but failed at reproducing an accurate magnetic field. A simpler model was then used, that allowed for more up to date and therefore, more accurate magnetic field predictions. By plotting the results of this new model on top of images of the Sun, the solar wind measured by Probe was classified by its source region on the solar surface, without any knowledge of plasma properties or composition. Such a technique was used to conclude that Probe was connected to a small coronal hole during its first perihelion. This, paired with Probe's unique orbital speed, which matched the rotation of the Sun, allowed for unprecedented localisation of the solar wind's source region to be demonstrated. This was explicitly quantified with the estimated speed of the magnetic footpoints dropping to an average of 130 ± 80km/h around a 2 week period at perihelion, perhaps changing how researchers should view the new Probe data.

A significant insight of this slow tracking speed was the discovery of patchy and quiet regions in Probe's magnetic field data, something that has never been observed in spacecraft data before. The average length scale of these regions were estimated as 600km and 200km for the patchy and quiet regions respectively. A suggested origin for these regions was explosive releases of particle jets from the edges of granules on the surface of the Sun, which themselves have a length scale of around 1000km.

In the future the peak's contribution to the acceleration of the solar wind can be quantified, by pairing these results with other Probe data concerning the speed and density of the solar wind particles. This would help trace the flow of energy in the Sun's atmosphere, which was highlighted as a main science goal of the Parker Solar Probe.

Contents

List of Figures

List of Tables

Chapter 1

Introduction

Out of the 10^{22} stars in the observable universe (ESA 2019), the Sun is the only star that we as a species can study in detail with in situ observations from spacecraft. High resolution data presents the opportunity to gain a better understanding of fundamental processes in our universe, that cannot be recreated in laboratories on Earth.

Biermann's (1957) observations of comet tails initially led to the idea of corpuscular radiation flowing outwards from the Sun. Parker then demonstrated the theory of a radially expanding gas outwards from the Sun, which was later coined the 'solar wind' (Parker 1958a; Parker 1958b). First evidence of this concept was presented by Soviet spacecraft (Gringauz et al. 1960), with the Mariner 2 spacecraft providing the categorical evidence of the solar wind's existence (Neugebauer and Snyder 1966, Parker 2001). Since then, the solar wind has been measured in situ by a number of spacecraft: to a distance of 63 solar radii, $R_{\odot}$, by Helios 1 and 2 (Porsche 1977); above the poles by Ulysses (McComas, Riley, et al. 1998); and is currently being measured just ahead of Earth by ACE (Stone et al. 1998) and WIND (Ogilvie and Parks 1996). These measurements, paired with remote sensing observations, such as those from the Solar and Heliospheric Observatory (SOHO) (Domingo, Fleck, and Poland 1995), have increased our knowledge of the solar wind's structure and origin. However, there are still many unresolved questions in heliophysics that can only be answered by sending scientific instruments close to the Sun (McComas, Velli, et al. 2007). This has been a high priority in space physics for many years, although technology has not allowed such a mission to exist until now.

The Parker Solar Probe (Probe) represents a new era for space physics, with a final perihelion only $9.86R_{\odot}$ from the Sun (Fox et al. 2016, pg.7). Probe was launched on the 12^{th} August, 2018, embarking on a 7 year mission which will consist of 24 orbits. This spacecraft aims to increase our understanding of the solar wind's formation and acceleration, by capturing high resolution data at unprecedented proximity to the Sun. The first perihelion for Probe took place in November 2018 with the spacecraft only $35R_{\odot}$ from the Sun, almost half the previous record held by the Helios spacecraft.

The initial aim of this project was to provide predictions of the solar wind conditions to be experienced by Probe. It was hoped that such predictions could be used to complement the in situ measurements taken by Probe, by providing global context. The accuracy of these predictions would then be evaluated, followed by an investigation into how potential shortcomings could be rectified with a modified ap-

proach. A secondary aspect of these predictions was to link Probe's measurements to features on the Sun, in order to study how the solar wind is generated and evolves out into interplanetary space.

The first orbit would not only provide the closest measurements of the Sun to date, but would also allow for a prolonged study of the solar wind's source region. This rare opportunity occurs when the spacecraft speed matches the rotation of the Sun, thus allowing Probe to investigate temporal as well as spatial structures in the solar wind. Such an opportunity has never been possible before with previous spacecraft, due to the high orbital velocities required. Therefore, initial objectives relating to this part of the project were deliberately left open-ended, although significant effort focussed on utilising this aspect of the Probe mission.

1.1 Magnetic field of the Sun

The structure and dynamics of the Sun are dominated by the intense magnetic field created by the turbulent plasma in the convection zone, known as the solar dynamo (Charbonneau 2010). Historic observations revealed that there is an 11-year cycle in solar activity between maximum and minimum (Arlt 2011). At each solar minimum, the Sun's magnetic field represents a dipole configuration, which constitutes a stark contrast to a disorganised magnetic field at solar maximum.

The visible surface of the Sun, known as the photosphere, is dominated by granules (see Figure 1.1a), which have an average length scale of ~ 1300 km and a lifetime of $8 - 15$ minutes (Javaherian et al. 2014). Here thermal pressure dominates over magnetic pressure, meaning that convective motion of the granules drags the magnetic field towards the darker intergranular lanes. This concentrates the magnetic field, which can appear as photospheric bright points in visible light observations (Keys et al. 2013).

The outer layer of the solar atmosphere, known as the corona (Cranmer and Winebarger 2018), is dominated by a strong magnetic field, that can exhibit stable large scale structures. One such feature, known as a coronal hole, can be seen as the darker region in Figure 1.1b. These are defined as open magnetic field lines that extend far into interplanetary space, containing cooler, less dense material which leads to its darker colour. These holes are often found, but are not limited to, high latitudes on the Sun at solar minimum (Habbal et al. 1997), as a consequence of a predominant magnetic dipole configuration.

Figure 1.1b also displays active regions as bright magnetic field loops in the corona, whose footpoints appear as sunspots on the photosphere. Active regions are the primary source of transient magnetic field events (Driel-Gesztelyi and Green 2015), with the largest being a coronal mass ejection, a violent eruption of plasma material from the corona (Webb and Howard 2012). These transient features can drive space weather at Earth, that can interfere with modern technology (Eastwood et al. 2017).

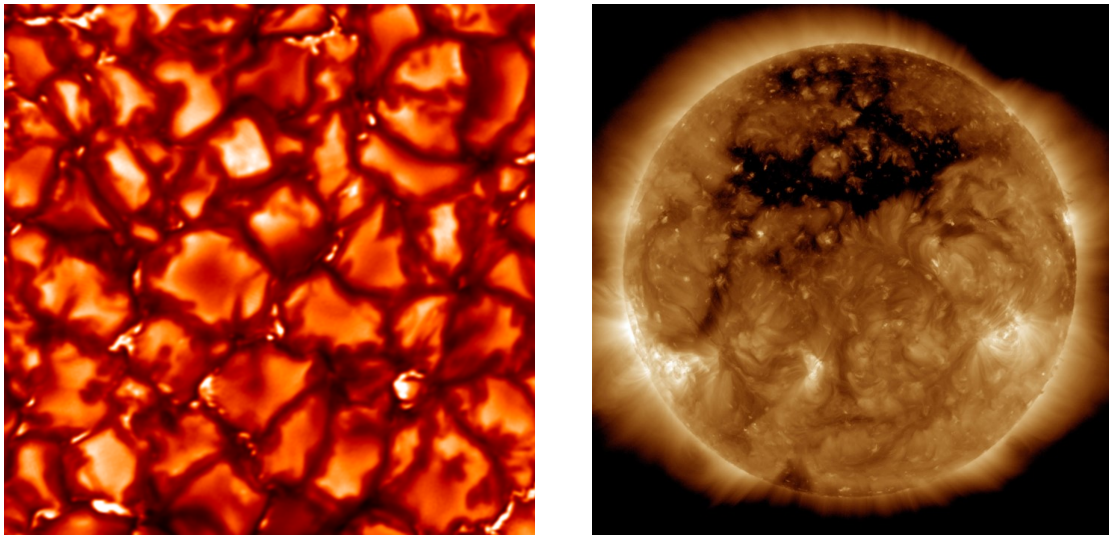

(a) (b)

Figure 1.1: *(a) shows the pattern of granules of the photosphere, which are a manifestation of convective motion below this surface. Photospheric bright points are visible in the some of the dark intergranular lanes (image retrieved from Henriques 2010).*
(b) image taken by the SDO spacecraft in at a wavelength of $193\mathring{A}$ *on the* 10^{th} *October 2015. A large coronal hole can be seen in black, where cooler material escapes from open field lines. Active regions are visible as brighter loops, where there is increased magnetic activity (image retrieved from NASA/SDO 2015).*

1.2 The Solar Wind

1.2.1 Interplanetary Magnetic Field

The solar wind is a highly conducting plasma expanding outwards from the corona at supersonic speeds (Schwenn and Marsch 1990, pg. 1), and consists mainly of protons with approximately $1\% - 5\%$ alpha particles and trace amounts of other heavier ions (Bochsler 2007). The solar wind extends throughout the solar system, creating a bubble-like cavity in the interstellar medium, known as the heliosphere. A consequence of the high conductivity is that the magnetic field lines in the plasma are said to be frozen in, meaning that they follow the motion of the plasma. Therefore, as the solar wind flows radially outwards from the Sun, it drags the interplanetary magnetic field (IMF) with it. This effect, paired with the rotation of the Sun, causes the magnetic field to take an Archimedean spiral shape, known as the Parker spiral (Parker 1958b).

The IMF can either point away (positive polarity) or towards (negative polarity) the Sun. Early observations revealed regions of constant polarity in the ecliptic plane (plane in which the Earth orbits the Sun), with reversals in polarity occurring two or four times per solar rotation (Smith 2001). A dominant polarity effect was also observed in latitude (Rosenberg and Coleman 1969), leading to the idea of a heliospheric current sheet (HCS) separating the two polarities. This, along with the Sun's tilt, means that a spacecraft orbiting in the ecliptic plane will cross the HCS,

with each crossing resulting in a change of polarity in the IMF. To be consistent with the Parker spiral, the HCS takes the form of a ballerina skirt as suggested by Alfvén (1977).

1.2.2 Solar Wind Structure and Origin

The solar wind has a two part structure, with a steady fast wind with speeds typically $> 600 kms^{-1}$ and a dense, more variable, slow wind with average speeds of $< 400 kms^{-1}$ (Schwenn 1983). Ulysses observed fast wind as it orbited above the poles of the Sun, with the results at solar minimum in Figure 1.2a. This demonstrates a well defined three dimensional structure with slow wind limited to low heliographic latitudes and fast wind dominant at higher latitudes (McComas, Riley, et al. 1998). Two distinct polarities can also be seen, mirroring the dipole structure of the Sun at solar minimum. However, this well defined structure to the solar wind is not apparent at solar maximum, with an intermediate wind speed at all latitudes (McComas, Elliott, et al. 2003), as seen in Figure 1.2b.

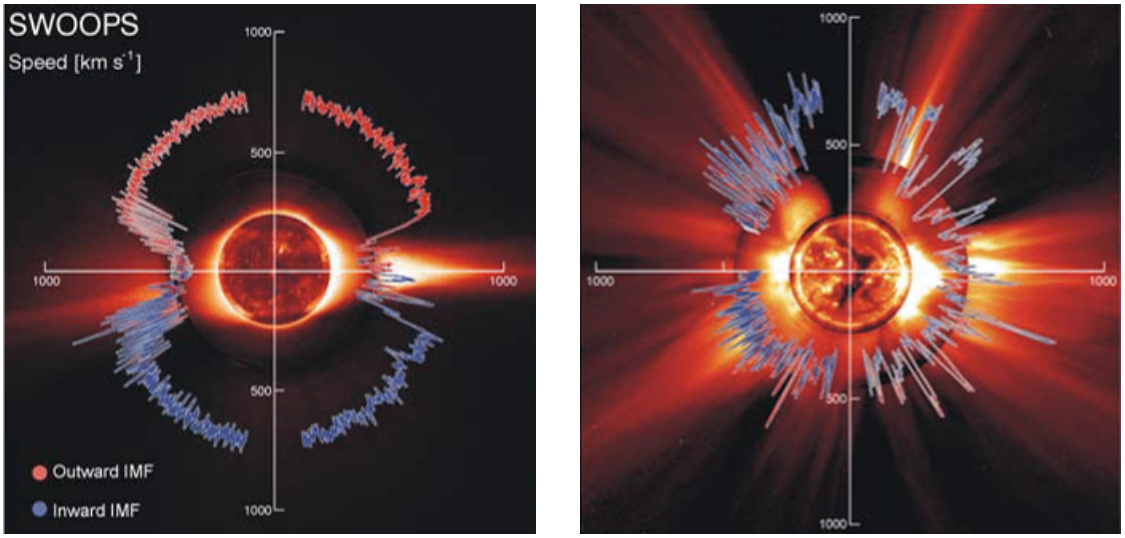

(a) *Solar Minimum* (b) *Solar Maximum*

Figure 1.2: *Shows polar plots for the angular distribution of velocities in the solar wind at solar minimum, (a), and maximum, (b), as measured by the Ulysses spacecraft. A clear structure can be seen at solar minimum, with slow wind only from low latitudes, whereas, at solar maximum, there is no clear distinction between slow and fast wind (image retrieved from McComas, Elliott, et al. 2003).)*

It is well established that fast wind originates from large coronal holes (Sheeley, Harvey, and Feldman 1976; Cranmer 2009), and the area of a coronal hole is positively correlated to the solar wind speed (Tokumaru et al. 2017; Verbanac et al. 2011). However, the source region and physical mechanism for the release of slow solar wind is not well defined. Differences in composition and variability have led to the idea that slow wind is released intermittently from areas outside of coronal holes, such as the active regions in Figure 1.1b (Rouillard et al. 2010; Abbo et al. 2016). An alternative view, is that slow wind can continuously flow from the edges of coronal holes, streaming along open magnetic field lines in a similar way to fast wind (Wang and Sheeley 1990; Schwadron et al. 2005; Wang, Ko, and Grappin 2009).

There is evidence that suggests slow wind can exhibit similar properties to fast wind (D'Amicis and Bruno 2015), particularly the presence of Alfvén waves (transverse magnetic field perturbations) (Alfvén 1942), leading to many modern efforts to categorise the solar wind other than by a simplistic cut in velocity. Many such categorisations aim to link in situ measurements to source regions on the Sun, using plasma properties (Stansby, Horbury, and Matteini 2019) and machine learning techniques (Camporeale, Carè, and Borovsky 2017). When grouped into slow and fast wind, these types of solar wind are mixed together, which can interfere with scientific results.

1.2.3 Coronal Heating and Solar Wind Acceleration

One of the most famous unanswered questions in space physics is that of the coronal heating problem, which was discovered in the first half of the 20^{th} Century (reviewed by Noci 2002). The heating problem manifests as temperatures of 6000K in the photosphere and 2×10^6K in the corona, even though the hotter corona is further from the energy source in the core (Dunbar 2012). McComas et al. (2007) states that the energy for this temperature gradient must be from convection in the photosphere, with the deposition process being the target of research efforts. The acceleration of the solar wind also requires large energy deposition, so can be considered as a byproduct of the coronal heating problem (Schwenn and Marsch 1990, pg.52). The longstanding nature of this problem means that various heating mechanisms have been proposed (Kuperus, Ionson, and Spicer 1981; Cranmer and Winebarger 2018), but no consensus has yet been reached.

One of the most popular theories is that the heating is due to ion-cyclotron resonance, which occurs when low frequency Alfvén waves resonantly interact with coronal ions (Isenberg 2001). These Alfvén waves can be launched as a consequence of the convective motion in the photosphere, and survive into the lower corona, where they can dissipate their energy (Kasper, Lazarus, and Gary 2008; De Pontieu et al. 2009).

Small scale magnetic reconnection has also been suggested to heat the corona (Parker 1988). This process of magnetic reconnection is ubiquitous throughout space plasma, where the rearranging of magnetic fields releases kinetic and thermal energy in well defined jets (Priest, Forbes, and Cambridge University Press. 2000; Biskamp 2000). Kasper et al. (2016) note that magnetic fluctuations have not yet been measured at small enough scales to investigate this possibility, although models suggest that robust scaling laws should be seen (Georgoulis, Velli, and Einaudi 1998).

1.3 Space Measurements

Before the launch of Parker Solar Probe, the Helios mission held the record for the closest distance to the Sun, at around 0.29AU. This mission consisted of two identical spacecraft, Helios A and B, which were launched around a year apart in December 1974 and January 1976 respectively (Schwenn and Marsch 1990, pg. 4). The last of this data was received in 1986, which was a period of solar minimum, as is also the case for the 7 years of Probe's mission.

This mission carried two flux-gate magnetometers, with a maximum data rate of 4 vectors/second (Ivory 1999). This technology was simple and robust, able to

survive the launch into space, and the years of bombardment from energetic particles. Consequently, this instrument design is still widely used, and features on Probe.

A fluxgate magnetometer design consists of a drive coil wrapped around a highly permeable core in a symmetric shape (see Figure 1.3). Current is then applied to the coil, driving the core material in and out of saturation. With no external magnetic field, there is an equal and opposite magnetic flux from each side of the core, meaning no change of flux in total. However, when there is an external field present, one side of the core comes out of saturation earlier, leading to a change in the flux, which induces a current that can be measured (Ness 1970). By combining three of these coils, a magnetic vector can be obtained. It is common for magnetometers to be placed on a boom away from the spacecraft, so as to avoid interference from the spacecraft's electronics.

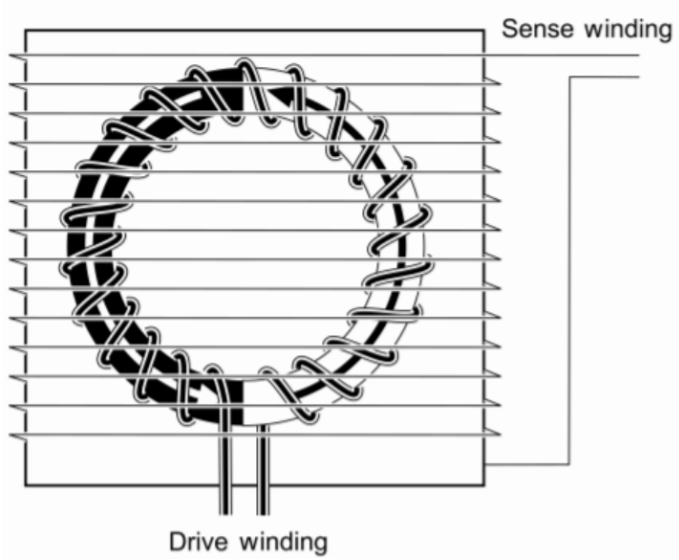

Figure 1.3: *Schematic of a typical fluxgate magnetometer instrument. A drive winding drives the permeable core in and out of saturation, whilst the sense winding measures any induced current from an external magnetic field. (diagram retrieved from Miles et al. 2017).*

1.3.1 Parker Solar Probe Instrumentation

Probe represents a major step forward in space physics, with the primary scientific objectives to (Fox et al. 2016, pg.10):

- Determine the structure and dynamics of the Sun's magnetic field
- Understand how the corona is heated and solar wind is accelerated
- Investigate how energetic particles are accelerated and transported

In order to meet these scientific objectives, Probe is equipped with four instrument suites: the Electromagnetic Fields Investigation (FIELDS); the Integrated Science Investigation of the Sun, Energetic Particle Instruments (ISIS); the Solar Wind Electrons Alphas and Protons Investigation (SWEAP); and the Wide Field Imager

for Solar Probe Plus (WISPR). For the purposes of this project, only the magnetic vector data from the FIELDS suite was available, therefore, further discussion will be restricted to this set of instruments.

The layout of the FIELDS instrument in shown in Figure 1.4, which consists of five electric field antennas, two fluxgate magnetometers and a search coil magnetometer. The latter measures the alternating changes in magnetic field, through the current induced by Faraday's law (Hospodarsky 2016). This is useful for measuring properties of plasma waves and turbulence. However, the focus of this project was the magnetic field vectors, which were provided by the fluxgate magnetometers. These can measure 292.97 vectors/second, with a large dynamic range (up to $\pm 63,536$nT), so as to allow the investigation of low amplitude fluctuations from turbulence and waves, and also the large increase in magnetic field from coronal mass ejections (Bale et al. 2016).

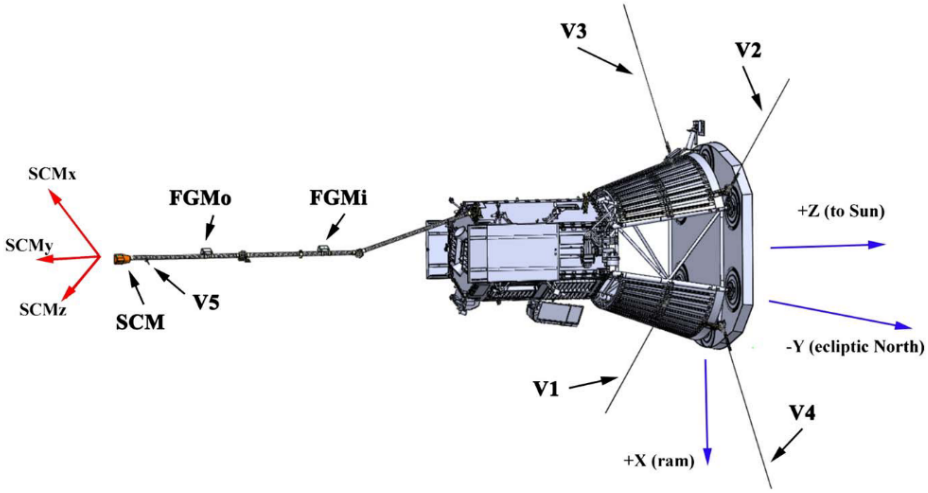

Figure 1.4: *Shows the layout for the FIELDS instrument suite aboard Probe. The five electric field antennas are labelled V1-5. The spacecraft always orients itself so that it points directly at the Sun, shielding the instruments behind. The two fluxgate magnetometers are labelled as FGMo (outboard) and FGMi (inboard). (diagram retrieved from Malaspina et al. 2016).*

Chapter 2

Methods Employed

2.1 Parker Solar Probe Orbit

The orbital details of any planetary body or spacecraft is handled with NASA's `SPICE` toolkit, developed at the Navigation and Ancillary Information Facility (NAIF) (Acton 1996; Acton et al. 2018). As this toolkit is written in `C`, a `Python` wrapper, `SpiceyPy` (Annex et al. 2019), was utilised. Due to the versatility of `SPICE` each specific spacecraft has its own 'kernels', which are files that define the spacecraft's clock, predicted position, orientation etc., as well as defining the relevant coordinate systems for the mission. Originally, these were downloaded manually[1], although later, `HelioPy` (Stansby, Rai, et al. 2018) was employed for its ability to automatically handle new kernels.

Transforming between different coordinates frames is essential throughout space physics research. As such, there exists well established packages such as `SunPy` (Mumford et al. 2019) and `AstroPy` (The Astropy Collaboration et al. 2018) that were used in this project to handle different frames, as well as mixing of units.

2.1.1 Carrington Coordinates

A commonly used inertial frame is named ECLIPJ2000, which has its x and y vectors lying in the same plane as the Earth's orbit (the ecliptic plane). This frame is useful for visualising Probe's orbit with respect to the planets, where multiple 'Venus gravity assists' over the mission duration bring Probe closer and closer to the Sun.

However, for the purposes of the report, it is more useful to consider a frame that rotates with the Sun. Such a frame is represented by Carrington Heliographic coordinates, where each point on the Sun's surface is given a Carrington longitude (Φ) and latitude (Θ). Originally, this was only for tracking sunspots on the Sun's surface (Carrington 1853; Ulrich and Boyden 2006), but can easily be extended to 3D by adding a radius (r). This frame rotates at the mean solar rotation rate: 25.38 days. Every time the central meridian of these coordinates aligns with the central meridian seen from Earth, a new Carrington cycle is started. The first of these cycles started on 9^{th} November 1853 and occur every 27 days, due to Earth also orbiting the Sun (Thompson 2006). Each cycle, the longitude viewed by Earth

[1] https://sppgway.jhuapl.edu/ancil_products

Carrington Cycle	Start Date	End Date
2208	2018 Sep 02	2018 Sep 29
2209	2018 Sept 29	2018 Oct 26
2210	2018 Oct 26	2018 Nov 23
2211	2018 Nov 23	2018 Dec 20

Table 2.1: *Shows the start and end date for the relevant Carrington Cycles (Retrieved from Lasley 2016)*

decreases from 360° → 0° before the next cycle starts. For context, Table 2.1 shows the relevant Carrington cycle numbers and dates for this project.

Figure 2.1a shows the inner solar system (excluding Mercury for clarity) for Probe's first perihelion in inertial coordinates, whereas Figure 2.1b shows the same situation in Carrington coordinates. In inertial coordinates, Probe and the planets orbit anti-clockwise, whereas, due to the Sun's superior rotation rate in Carrington coordinates the orbital direction is clockwise. The small loop created by Probe at perihelion in Figure 2.1b is a result of Probe travelling slightly faster than the Sun's surface, so that in Carrington coordinates it travels anti-clockwise for a few days, before returning to the usual clockwise direction.

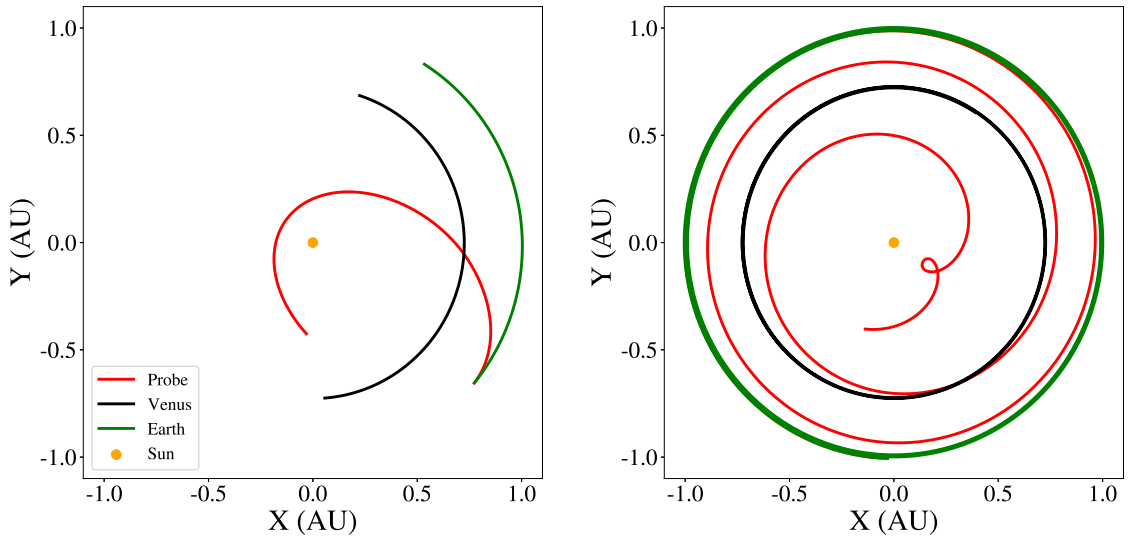

(a) *Inertial Frame* (b) *Heliographic Carrington Frame*

Figure 2.1: *(a) shows the orbits of Venus, Earth and Probe from the* 12^{th} *August 2018, to* 20^{th} *November 2018 in the ECLIPJ200 inertial frame.*
(b) shows the same orbits but in the Heliographic Carrington frame. The Venus gravity assist can also be seen in these graphs, where energy is actually transferred from Probe to Venus, reducing Probe's velocity meaning it can travel closer to the Sun.

2.1.2 Ballistic Mapping

This report frequently compares Probe's orbit to a solar wind profile in Φ and Θ at a constant radius, R_{surf}. In order to do this, Probe's orbit at various radii must

be mapped back to R_{surf} so that an accurate comparison can be made. This was achieved using ballistic mapping (Neugebauer, Liewer, et al. 2002), which makes the valid assumption that the solar wind flow is radial, as demonstrated in Figure 2.2.

Assuming the solar wind flow is radial with a constant speed, V_{sw}, the shift in longitude, $\Delta\Phi$, when at a radius, r, is defined as:

$$\Delta\Phi(r) = \Omega\left(\frac{r - R_{surf}}{V_{sw}}\right). \tag{2.1}$$

A speed of $V_{sw} = 360\text{kms}^{-1}$ was used throughout, as it represents a nominal solar wind speed. The solar wind speed will not always be this exact value, leading to an inherent uncertainty in this procedure, with changes in V_{sw} leading to a error of 5°.

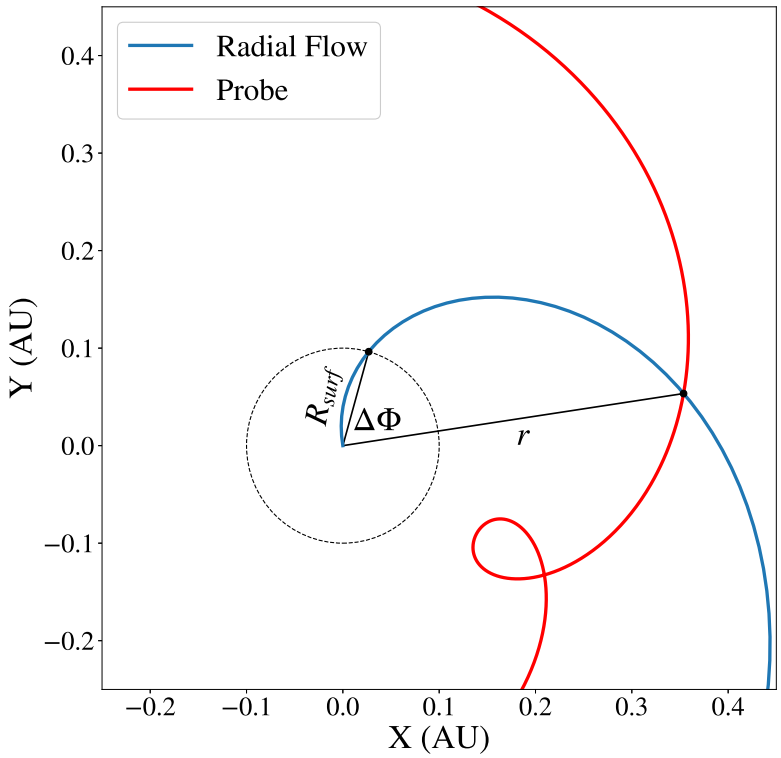

Figure 2.2: *Demonstrates how ballistic mapping is carried out for Probe's orbit along a radial flow. The spiral here is exaggerated to see more clearly how the mapping works; it does not represent a typical solar wind flow. The surface that is being mapped to is shown with the dotted black circle.*

2.2 Potential Field Source Surface (PFSS) Model

The Potential Field Source Surface (PFSS) model first originated in the 1960s as a method to model the large scale global structure of the corona (Altschuler and Newkirk 1969; Schatten, Wilcox, and Ness 1969).

This model assumes that the corona is both force and current free, which from Ampère's law means:

$$\nabla \times \vec{\mathbf{B}} = 0, \tag{2.2}$$

where $\vec{\mathbf{B}}$ is the magnetic field, and the displacement current has been neglected for a plasma. The solution to this equation is that of a scalar potential field, Ψ, such that:

$$\vec{\mathbf{B}} = -\nabla\Psi. \tag{2.3}$$

Combined with a divergent free magnetic field ($\nabla \cdot \vec{\mathbf{B}} = 0$), Ψ then satisfies Laplace's equation:

$$\nabla^2\Psi = 0, \tag{2.4}$$

where solutions to Laplace's equation in spherical coordinates are well known (Mackay and Yeates 2012). In order to simulate the corona, a condition that $\vec{\mathbf{B}}$ is radial at a spherical source surface of radius, R_{ss}, is enforced. Beyond this source surface, the magnetic field is assumed to behave as the Parker spiral from Section 1.2.1. The value of R_{ss} is considered a free parameter in the model, although it is common practice to set this equal to 2.5 solar radii, $R_\odot$, so as to match observations of the coronal magnetic field from solar eclipses (Hoeksema, Wilcox, and Scherrer 1983). Studies have investigated the effect of changing this source surface (Arden, Norton, and Sun 2014), however, for this project the standard value will be used.

A magnetic map (magnetogram) is used to provide the inner boundary condition at one $R_\odot$. These were provided hourly by the Global Oscillation Network Group (GONG) observatories[2], at 6 locations around the globe (Hill et al. 1994). The magnetic field strength is measured using the spectral split due to the Zeeman effect. This means that such measurements are line of sight, so only radial magnetic fields can be recorded. An important point to note is that, although GONG magnetograms represent the whole Sun's surface, they only update one degree of Carrington longitude at a time.

The PFSS solution was then solved using `PfssPy` (Stansby 2019), a `Python` package that builds on the finite difference methods set out by Yeates (2018).

The implementation of this package was validated by inputting a purely dipole magnetic field, where the radial component of the magnetic field obeys:

$$B_r = \frac{2sin(\Theta)}{r^3}, \tag{2.5}$$

where Θ is the latitude ($\Theta = 90°$ points straight up), and r is the radial distance. The output of the PFSS model for this dipole input can be seen in Figures 2.3a and 2.3b, demonstrating that the PFSS model behaves as expected.

This model has been widely used for over 40 years with a wide range of applications such as tracing the sources of solar wind (Neugebauer, Liewer, et al. 2002) and determining the background magnetic field in coronal mass ejections (Titov et al. 2017). However, this model cannot capture the effects of currents in the corona, which are present in twisted magnetic field structures, which have led to the development of non-potential models (Edwards et al. 2015).

[2] https://gong.nso.edu/data/magmap/

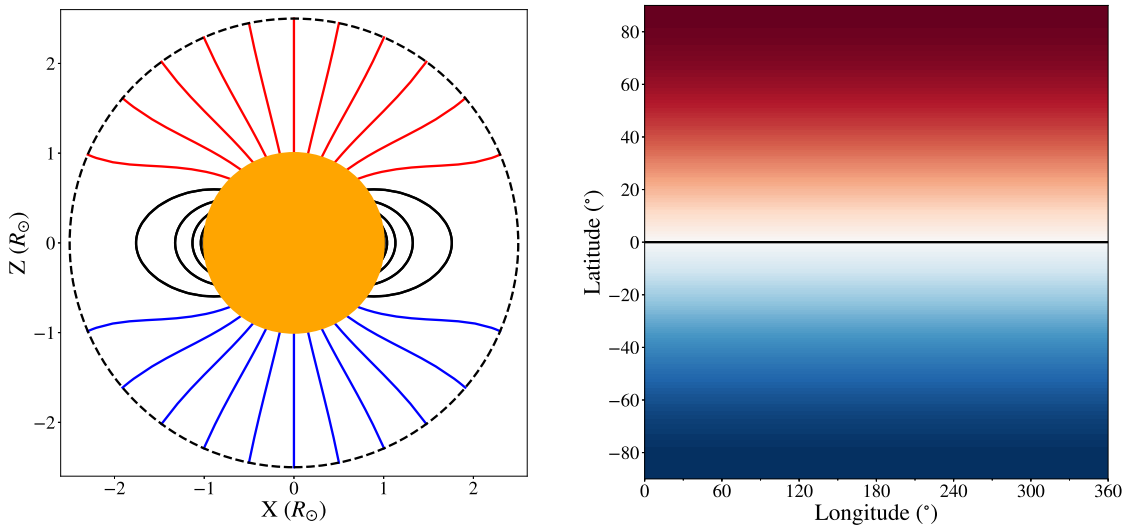

(a) (b)

Figure 2.3: *(a) The magnetic field lines from the PFSS model output are shown for a dipole field in two dimensions. Red and blue are open field lines of positive and negative polarity respectively. Black field lines are closed, so do not reach the source surface, represented by the dotted black circle.*
(b) Shows the output of the PFSS model at the source surface for a dipole field. The blue and red colours represent magnetic fields going in and out of the Sun respectively. The exact values are not relevant for this project, only the absolute polarity of the magnetic field. The black line representing the inversion between the two polarities.

2.2.1 Wang-Sheeley (WS) Model

It was discovered that solar wind speed at 1AU was inversely proportional to the rate of coronal flux-tube expansion (Wang and Sheeley 1990), defined as:

$$f = \left(\frac{R_\odot}{R_{ss}}\right)^2 \left(\frac{B_r(R_\odot)}{B_r(R_{ss})}\right), \tag{2.6}$$

where $B_r(R_\odot)$ is the radial magnetic field strength of the field line connecting the solar surface to the source surface, which has a radial strength of $B_r(R_{ss})$. The velocity of the solar wind, V_{WS} is then calculated as:

$$V_{WS} = V_0 + \frac{V_1 - V_0}{f^\alpha}, \tag{2.7}$$

where $V_0 = 267.5\text{kms}^{-1}$, $V_1 = 677.5\text{kms}^{-1}$ and $\alpha = 0.4$ (Arge and Pizzo 2000). This is the simplest model of solar wind velocity from purely magnetic field measurements, and does not take into account the size of coronal holes, and distance from the coronal hole boundary (Reiss et al. 2019).

2.2.2 Magnetic Connectivity

Using the PFSS model presents the opportunity to evaluate which magnetic field line connects Probe to the solar surface, with the potential to highlight the source region of the solar wind. To achieve this, Probe's trajectory is first ballistically

mapped back to the PFSS source surface at $2.5R_\odot$, using the technique described in Section 2.1.2.

The PFSS solution represents the magnetic field in all directions from $R_\odot \rightarrow R_{ss}$. The coordinates of the mapped trajectory on the source surface act as the boundary condition for an initial value problem, which is then solved with `Scipy`'s (Jones, Oliphant, Peterson, et al. 2019) integration package. More specifically the LSODA method was used which is based on Petzold (1983) and code written by Hindmarsh (1983). This then results in a field line connecting the source surface to the solar surface in heliographic Carrington coordinates.

The `Astropy` coordinate objects and `SunPy` defined frames were then used to transform this field line into a helioprojective frame, that is commonly used for images taken of the Sun. This meant that the field line could be directly plotted onto an image of the Sun, clearly demonstrating the solar origin of the field line.

Such images were downloaded using `SunPy`'s Helioviewer client, that was able to retrieve images from the STEREO-A spacecraft at a wavelength of 195Å. This spacecraft orbits ahead of Earth, delivering a more comprehensive view of the Sun's surface at any one time (Howard et al. 2008).

2.3 Magnetohydrodynamic (MHD) Model

The Community Coordinate Modeling Center (CCMC) is a multi-agency partnership, providing the scientific community with access to a wide range of space physics simulations[3]. These simulations are available for 'Runs-on-request', taking advantage of the large processing power available to complete the model, that would not be possible to many scientists without high powered computing facilities and technical knowledge. The model used for this report is known as the 'WSA-Enlil' model, which couples together several physics based models in order to simulate the inner heliosphere, and takes around a week to complete.

2.3.1 Wang-Sheeley-Arge (WSA) Model

The PFSS model, described in Section 2.2, was first used to extend the magnetic field of the corona out to $2.5R_\odot$. The inner boundary is provided by a magnetogram from the GONG observatory, averaged over a whole Carrington rotation.

The Wang-Sheeley-Arge model was then used, which includes some improvements on its successor, the WS model. The first improvement is the use of the Schatten current sheet model (Schatten 1972), that provides a more physical magnetic field topology out to $30R_\odot$. This additional modification includes the effects of current sheets in the corona, that were forbidden in the PFSS solution. The coupling of these two models is described by Arge et al. (2004).

The second improvement is to introduce two new parameters: θ, which represents the angular separation between the magnetic field footpoint and nearest coronal hole boundary; and w, which is the width over which the wind speed reaches coronal hole values (Reiss et al. 2019).

[3] https://ccmc.gsfc.nasa.gov/

This then gives the solar wind velocity according to:

$$V_{WSA} = V_0 + \frac{V_1 - V_0}{(1+f)^\alpha}\left(\beta - \gamma \exp(-(\theta/w)^\delta)\right)^3, \tag{2.8}$$

where f is the expansion factor defined in Equation 2.2.1. Additionally, α, β, γ and δ are all parameters that are empirically fine tuned for the CCMC standard model. Assuming momentum flux conservation and thermal balance, this model can also calculate the density and temperature at $30R_\odot$ (Jian, Russell, et al. 2011). The WSA model is widely used due to its applications in space weather forecasting, as it provides a simple and reliable prediction of solar wind velocity (Sheeley Jr 2017).

2.3.2 Enlil

The output of the WSA model is then used as an inner boundary condition for a large scale magnetohydrodynamic (MHD) model known as Enlil. MHD models such as this one treat the plasma as a fluid, where macroscopic variables of which are calculated using the magnetic fluid equations for conservation of mass, momentum and energy (Odstrcil 2003):

$$\frac{\partial \rho}{\partial t} + \nabla \cdot (\rho \vec{\mathbf{u}}) = 0, \tag{2.9}$$

$$\rho \frac{\mathrm{d}\vec{\mathbf{u}}}{\mathrm{d}t} = -\nabla P_{th} - \nabla\left(\frac{\vec{\mathbf{B}}^2}{2\mu_0}\right) + \frac{1}{\mu_0}\left(\vec{\mathbf{B}} \cdot \nabla\right)\vec{\mathbf{B}} + \vec{\mathbf{F}_{\mathbf{grav}}}, \tag{2.10}$$

$$\frac{\partial}{\partial t}\left(\frac{P_{th}}{\gamma - 1}\right) + \nabla \cdot \left(\vec{\mathbf{u}}\frac{P_{th}}{\gamma - 1}\right) = -P_{th}\nabla \cdot \vec{\mathbf{u}}, \tag{2.11}$$

where $\vec{\mathbf{u}}$ is the bulk plasma velocity, ρ is the mass density, $\vec{\mathbf{B}}$ is the magnetic field, $\mathbf{F_{grav}}$ is the gravitational force of the Sun, μ_0 is the permeability of free space, P_{th} is the thermal pressure and γ is the ratio of specific heats.

These can be coupled with the magnetic induction equation:

$$\frac{\partial \vec{\mathbf{B}}}{\partial t} = \nabla \times \left(\vec{\mathbf{u}} \times \vec{\mathbf{B}}\right), \tag{2.12}$$

which represents ideal MHD, with no diffusion of the magnetic field. These set of equations can then be closed by considering the total energy density, U, as the sum of thermal, kinetic and magnetic energy densities:

$$U = \frac{P_{th}}{\gamma - 1} + \frac{1}{2}\rho\vec{\mathbf{u}}^2 + \frac{\vec{\mathbf{B}}^2}{2\mu_0}. \tag{2.13}$$

Enlil solves these equations in three dimensions using a Total-Variation-Diminishing Lax-Friedrich scheme (Tóth and Odstrčil 1996). The condition that the magnetic field is divergence free ($\nabla \cdot \vec{\mathbf{B}} = 0$) is enforced using a field-interpolated central difference method (Tóth 2000). An azimuthal component to the magnetic field is added at $30R_\odot$, which is just the deflection from radial direction along the Parker spiral due to the local radial plasma velocity, and the meridional component is assumed to be zero.

The implementation of GONG, WSA and Enlil at CCMC has been validated by Jian et al. (2015), which states that this model captures the time series of normalised solar wind parameters well. Although, it is also mentioned that this model severely underestimates the strength of the magnetic field, by up to 80%.

Riley et al. (2006) compared the PFSS model to MHD models, concluding that the PFSS model can be implemented more easily, and under the right conditions can be a useful tool for reconstructing coronal structure. However, the MHD models are based on more physical assumptions and can be used to model coronal mass ejections (Pizzo et al. 2011) and have the potential to incorporate time dependent boundary conditions.

Chapter 3

Results and Discussion

3.1 Comparing Models to Data

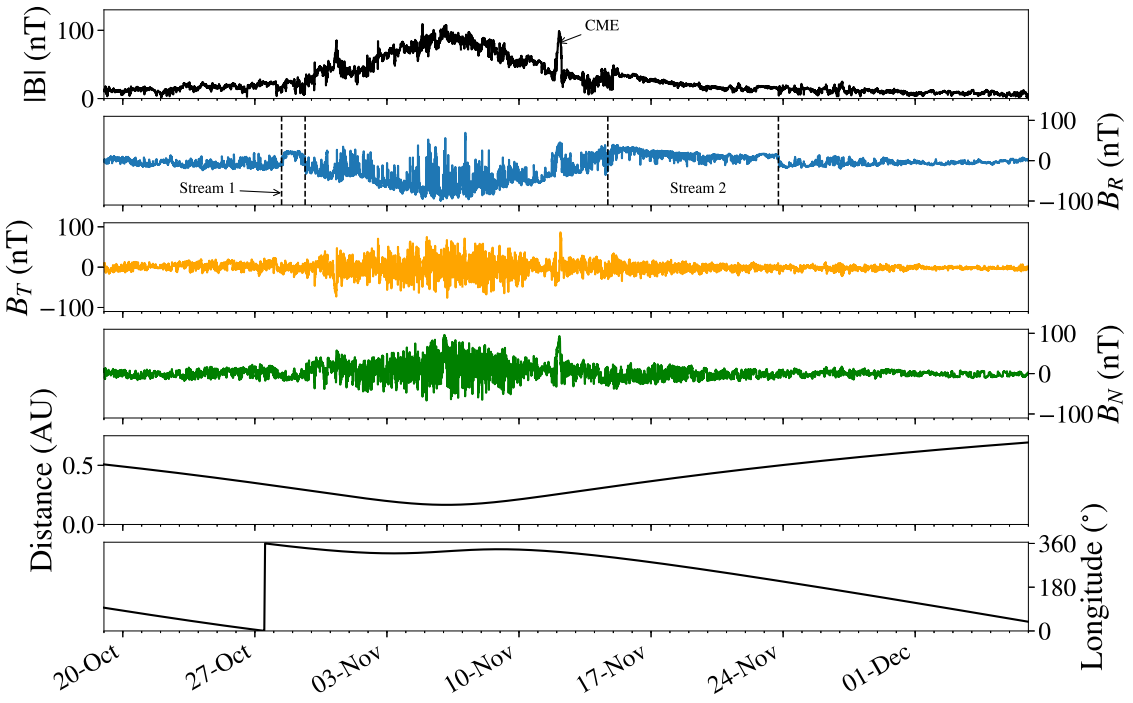

Figure 3.1: *Overview of the magnetic field data that was measured by Probe on its first orbit, and used throughout this project. This overview shows a five minute average of data for clarity, with the distance to the Sun and Carrington longitude shown in the bottom two axes. The large increase in magnetic field strength on the* 12^{th} *November was identified as a Coronal Mass Ejection (CME). Positive polarity regions, to be referred to as stream 1 and 2, are shown with pairs of dotted lines on the* B_R *axis.*

Figure 3.1 shows an overview of the magnetic field data available from Probe's first encounter in October and November 2018, with perihelion occurring on 6^{th} November. The data in this project has a rate of 10Hz when Probe was below 0.25AU, and 2Hz when further than this distance threshold. The Radial Tangential

Normal (RTN) coordinate system was used for this magnetic field data. R points from the centre of the Sun to the spacecraft, T is the cross product of heliographic polar axis and R, and N completes the right handed coordinate set (Fränz and Harper 2002).

The first important feature in this data is that the polarity of the magnetic field is predominantly negative (i.e. $B_R < 0$ nT), with a large positive polarity section between the 14^{th} and 23^{rd} November (stream 2), and a smaller region lasting from 28^{th} to 29^{th} October (stream 1). The ability to capture this global structure, using the models in Chapter 2, will be investigated in this section (3.1).

The magnetic field data is much more variable than that seen in other spacecraft data, with large fluctuations changing the polarity of the magnetic field. An investigation into the duration and distribution of these fluctuations is given in Section 3.2.

3.1.1 MHD Model

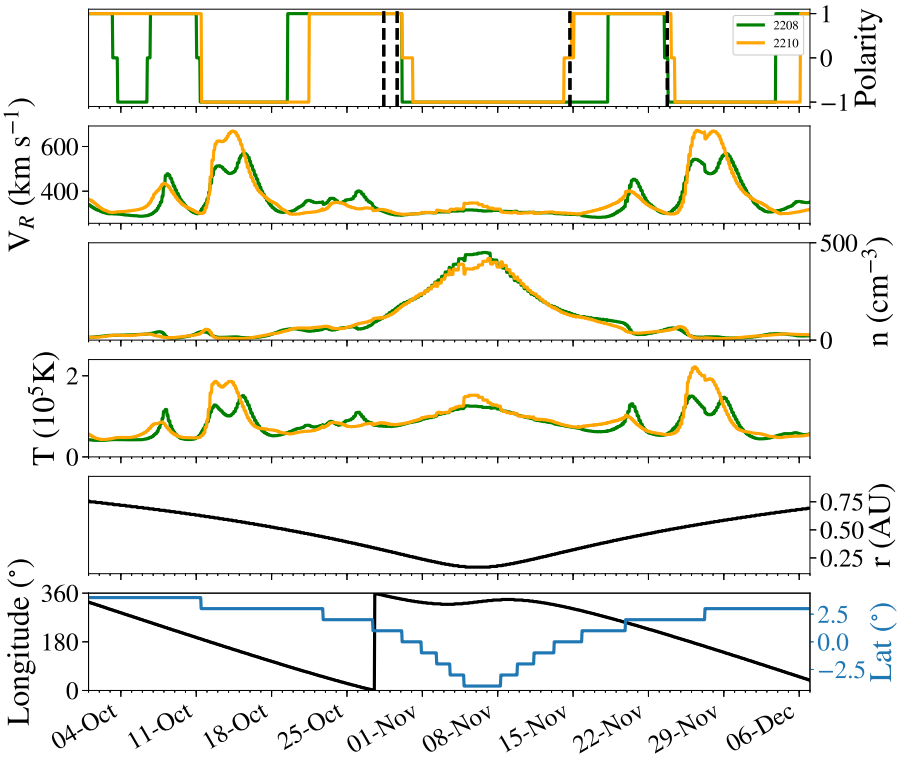

Figure 3.2: *Prediction for solar wind conditions sampled by Probe using MHD simulations for the 2208 and 2210 Carrington rotations (see Table 2.1 for the corresponding dates). The pairs of dotted lines on the polarity axis are the same as those seen in Figure 3.1. This indicates a consistent prediction of slow wind and negative polarity at perihelion in both simulations.*

One of the main aims of this project was to provide predictions ahead of time for the solar wind conditions that Probe would face on its first encounter with the Sun. The MHD model described in Section 2.3 was the first model employed, as

it allowed for the prediction of macroscopic solar wind variables such as number density (n), temperature (T) and radial speed (V_R). Probe data was downloaded from the spacecraft in December 2018, so simulations were run for the 2208 and 2210 Carrington rotations, with a confident prediction of negative polarity and slow solar wind at perihelion.

The results of these simulations are shown in Figure 3.2, with striking similarity between each simulation for the n, T and V_R profiles, even though they are two months apart. This highlights how stable features on the Sun are when at solar minimum, which is also demonstrated by the similarity, at low latitudes, of Figure 3.3a and 3.3b. A band of slow solar wind at low latitudes can be seen in both simulations, as well as a large, fast velocity stream at around 180°.

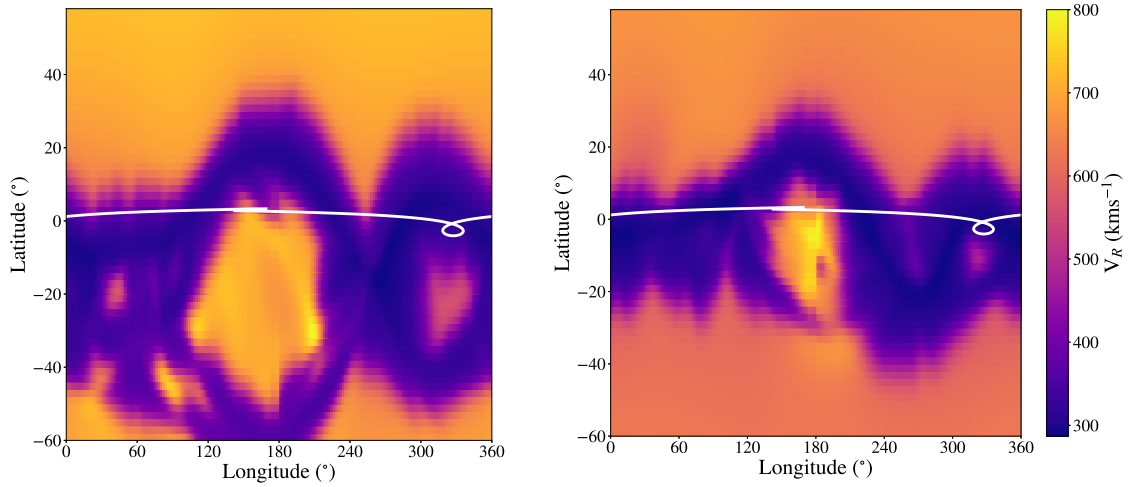

(a) *2208* (b) *2210*

Figure 3.3: *(a) solar wind velocity profile at 0.2AU for the MHD model using the 2208 Carrington rotation with Probe's orbit mapped back to 0.2AU (white line). (b) Shows similar for the 2210 Carrington rotation. This indicates little variation in solar wind speed at lower latitudes, where Probe orbits. However, large variations can be seen in higher latitude regions, though this is not relevant when predicting Probe's conditions. The colour bar represents both these plots.*

These simulations predict a negative polarity in the magnetic field at perihelion, which was observed as a negative B_R component in Figure 3.1, validating this method for solar wind prediction. The full global structure of the coronal magnetic field can be observed in Figures 3.4a and 3.4b for the 2208 and 2210 rotations respectively, with the colour of the line plot indicating the polarity observed by Probe. This shows good agreement with the magnetic field from Probe around perihelion for the 2210 rotation, especially for stream 2, although this stream was too narrow when using the 2008 model.

However, the MHD model fails to capture the position of the Heliospheric Current Sheet (HCS) between 0° and 80° longitude. This manifests as extra HCS crossings (when the polarity reverses) in Figure 3.2, which takes some credibility away from the correct current sheet predictions, such as those produced about stream 2. This suggests that an average magnetogram from a full Carrington rotation may not be able to confidently predict the magnetic field, and more up to date input data may be necessary.

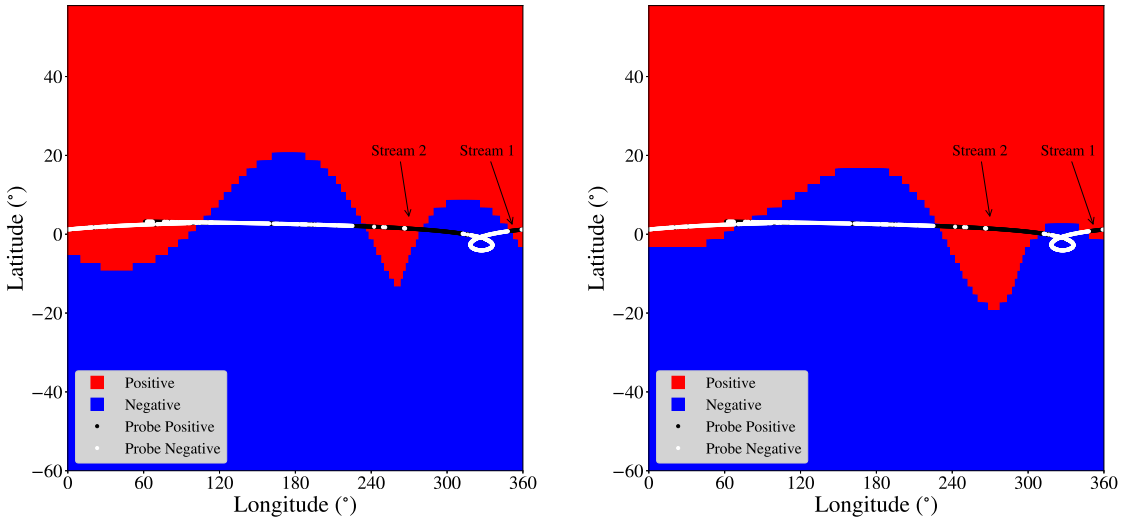

(a) *2208* (b) *2210*

Figure 3.4: *(a) solar wind polarity profile at 0.2AU for the MHD model using the 2208 Carrington rotation, with the line plot colour representing the polarity observed by Probe. A correct prediction can be seen at perihelion (the loop), but prediction of stream 2 is too narrow.*
(b) Shows a similar profile for the 2210 Carrington rotation. The 2210 simulation captures the negative polarity at perihelion and also successfully predicts the location of stream 2, around 270° *longitude. Although, it is not successful between* 0° *and* 80° *longitude.*

The MHD model considers the solar wind as a fluid, with added coupling to electric and magnetic fields. This means that it would be useful to compare the predictions to the n, T and V_R experienced by Probe, however, only magnetic field data was accessible.

To solve this problem, data was used from the Advanced Composition Explorer (ACE) spacecraft (Stone et al. 1998), located at the L1 Lagrangian point, which lies just ahead of Earth on the Sun-Earth line (Cornish 2019). This is equivalent to comparing with Probe data, since the solar wind that Probe experienced at perihelion then travelled out to 1AU, where it is sampled by the ACE, as seen in Figure 3.5.

This shows that the prediction of slow solar wind at perihelion was correct, with Probe passing through two high speed regions on either side. This successful radial speed prediction highlights the strength of the MHD model, that is well established in the literature (Owens et al. 2008; Jian, Russell, et al. 2011; Jian, MacNeice, et al. 2015; Reiss et al. 2019). The magnitude and pattern of velocity matches well, up until 15^{th} December when a fast stream is present in the ACE data only. It is believed that the steady state assumption of the Sun's velocity profile breaks down here, where a new coronal hole has appeared but is not represented in the magnetogram input. This, along with erratic polarity predictions in Figure 3.2, highlights the use of a Carrington average magnetogram as the primary weakness for this method, suggesting more up to date measurements were required. Another problem with this technique is that such a simulation has to be carried out at least a week in advance, due to the computationally expensive Enlil part of the model. The

timing of each Carrington rotation may not be optimal for Probe's future perihelia, so could potentially be several weeks out of date.

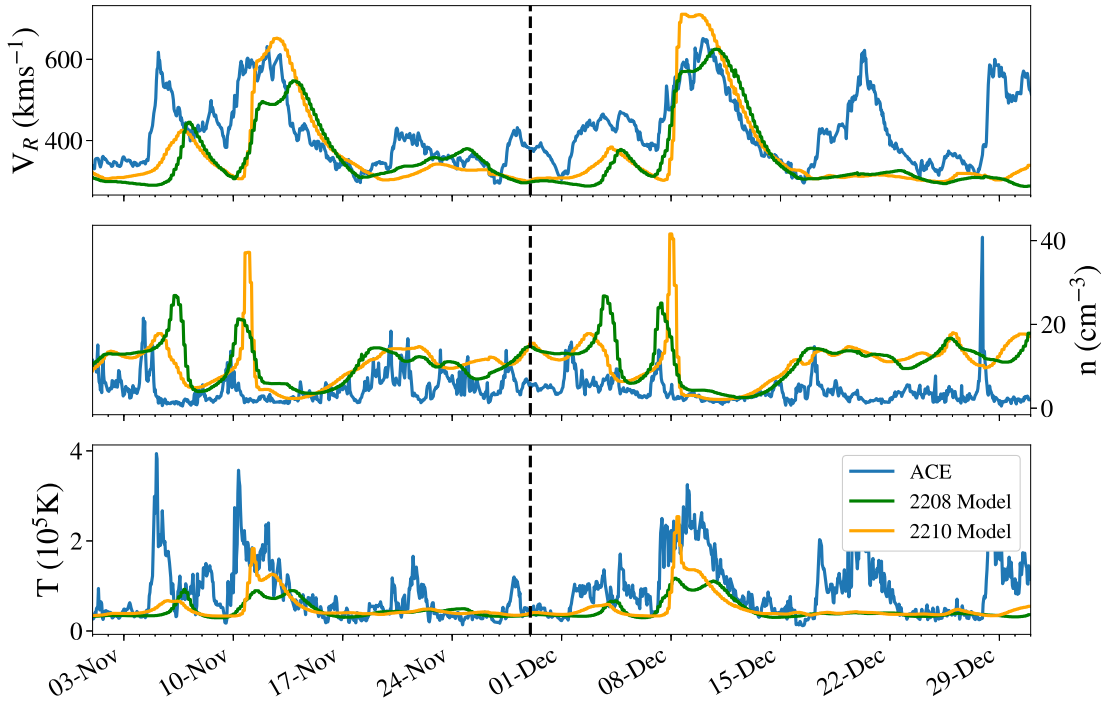

Figure 3.5: *Comparison of the 2208 and 2210 MHD model predictions at Earth, with data measured by the ACE satellite. The solar wind experienced by Probe at perihelion, on 6th November, then travelled radially outwards where it reached Earth on the date marked by the dotted black line. This shows the slow solar wind prediction was correct.*

3.1.2 PFSS Model

It was therefore decided to focus solely on the magnetic field prediction, using the PFSS model discussed in Section 2.2. The advantages of this model are that magnetograms were available from GONG every hour, and the PFSS model could be run in a few minutes on a standard computer. This meant a much more up to date structure of the coronal magnetic field could be created, with the added advantage of connecting Probe to a magnetic field line as described in Section 2.2.2. The shortcoming of this model is that it sacrifices the plasma properties that Enlil offers, although, as only magnetic field data was accessible for this project, this should not be considered a weakness.

The prediction of polarity and a solar wind speed, using the WS model in Section 2.2.1, is shown against the observed polarity in Figure 3.6. This corroborates with the MHD model, and observed properties, by anticipating negative polarity and slow solar wind at perihelion. Figure 3.6 also demonstrates a noteworthy accuracy in the positive polarity stream 2, which spanned from 14^{th} 17 : 00 to 23^{rd} 18 : 00 November in the Probe data. With a one hour time step, the PFSS model predicted a positive polarity stream between 14^{th} 18 : 00 and 23^{rd} 13 : 00.

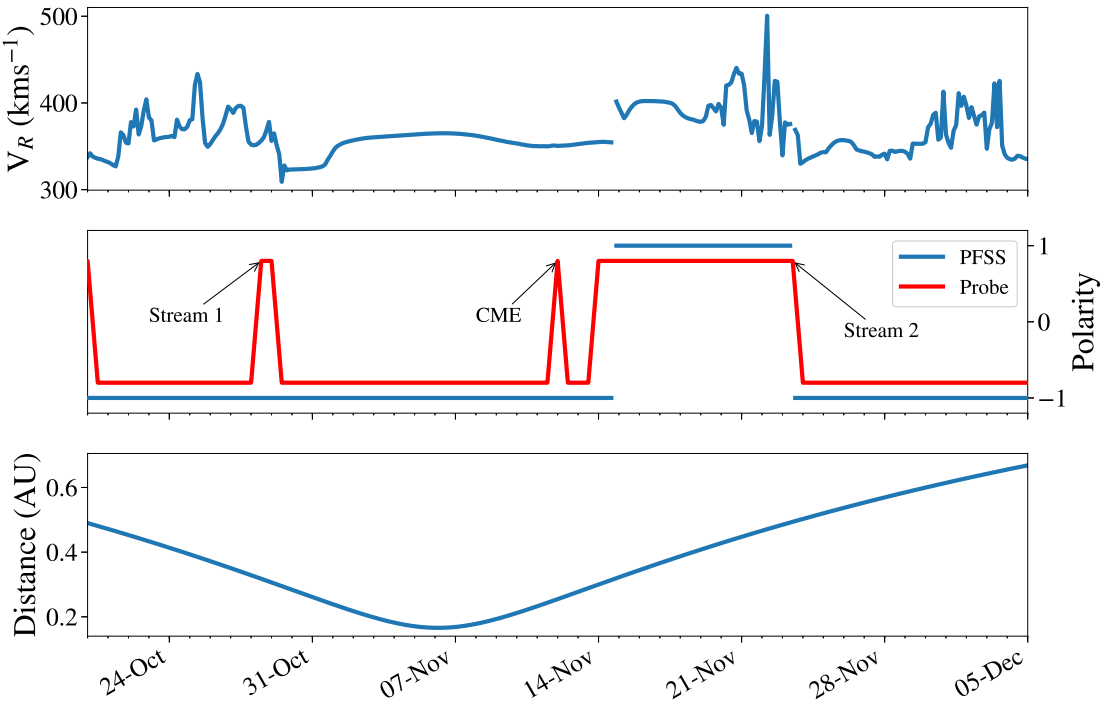

Figure 3.6: *Predicted solar wind speed and polarity every 3 hours using the PFSS model on a magnetogram from* 6^{th} *November. This is plotted against the actual polarity observed by Probe averaged over 12 hours (red), showing good agreement with the model, especially for stream 2 between* 14^{th} *and* 23^{rd} *November. The figure also shows faster solar wind from this positive polarity region, similar to that observed in the MHD simulations.*

The global structure of the coronal magnetic field at the source surface can be seen in Figure 3.7. Much like the 2210 MHD simulation seen in Figure 3.4b, this demonstrates an accurate shape of the positive stream after perihelion, but also provides a solid polarity prediction for all values of longitude. Therefore, unlike the MHD prediction, an accurate prediction of magnetic structure can be provided for the whole surface, without being undermined by inaccuracies in the HCS position.

There is a small HCS crossing between 28^{th} and 29^{th} October (stream 1), as seen in Figure 3.8, which was not predicted using a static magnetogram. However, the green line in Figure 3.7 shows the HCS for the 29^{th} October, highlighting how close Probe was to the HCS at this point in its orbit. There is no explicit change in magnetic polarity here when using the PFSS model, although it is reasonable to suggest that a small variation in the position of the current sheet could have led to a polarity reversal. It might have been the case that the current sheet moved over Probe, being changed by the appearance of a new active region, for example. Alternatively Probe may have passed through a static HCS that was slightly lower than in the PFSS model.

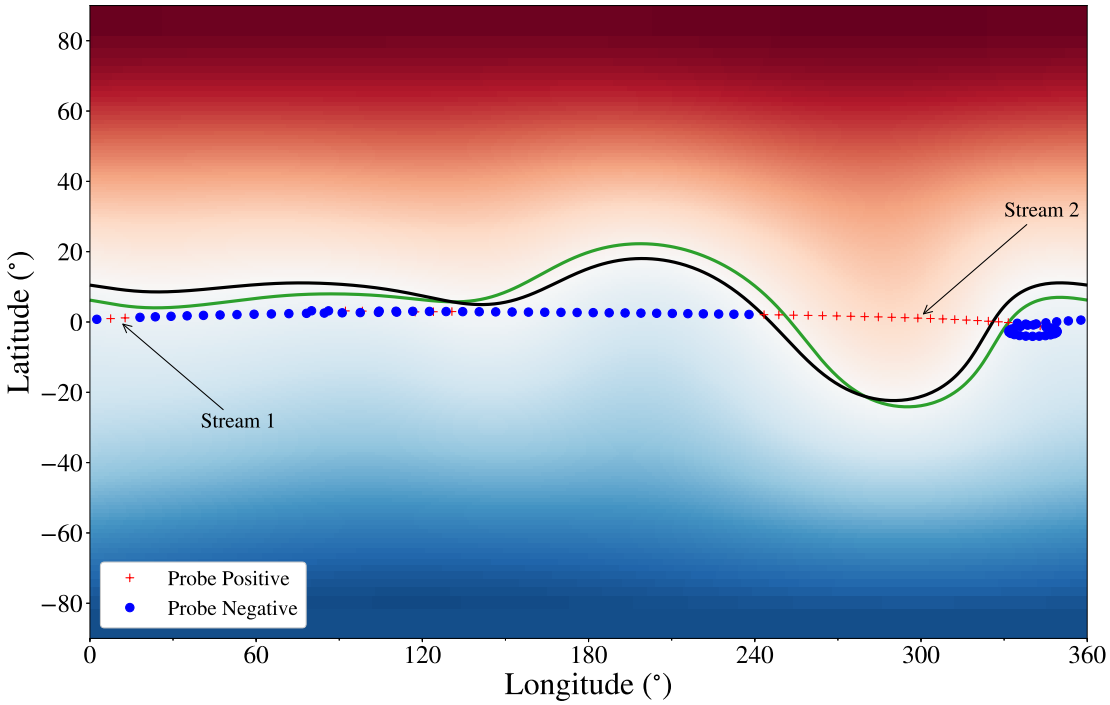

Figure 3.7: *Shows the PFSS model output at* $2.5R_{\odot}$ *using a magnetogram from* 6^{th} *November, with the HCS represented with the black line. The polarity of the magnetic field observed by Probe, averaged over 12 hours, is shown by each scatter point. This demonstrates how the PFSS model is effective at recreating the global magnetic structure of the corona. Stream 1 was not explicitly predicted by the model. lthough, the green line represents the HCS on the* 29^{th} *October, when this stream took place. The lower position of the HCS at this longitude suggests Probe could have switched polarity.*

Figure 3.8 shows that the initial transition from negative to positive polarity lasted 13 hours, while the reverse took only 5 hours. This asymmetry can not be explained by Probe passing through a static HCS of constant thickness, therefore, supporting the idea that the HCS moved over Probe.

The fluctuations in all three of the magnetic field components reduce between the two dotted red lines, which suggests a different solar wind flow. There is also a reduced magnetic field magnitude during this entire period, indicating the presence of a higher thermal pressure. This could be an observation of the heliospheric plasma sheet which envelopes the current sheet, and has a higher thermal pressure (Winterhalter et al. 1994). Studies observing this plasma sheet also exhibit drops in the field magnitude, arising from intermittent releases of hot plasma from closed field lines at the solar equator (Crooker et al. 2004). Such dips are seen in Figure 3.8, although particle density and temperature measurements are needed to fully verify this classification.

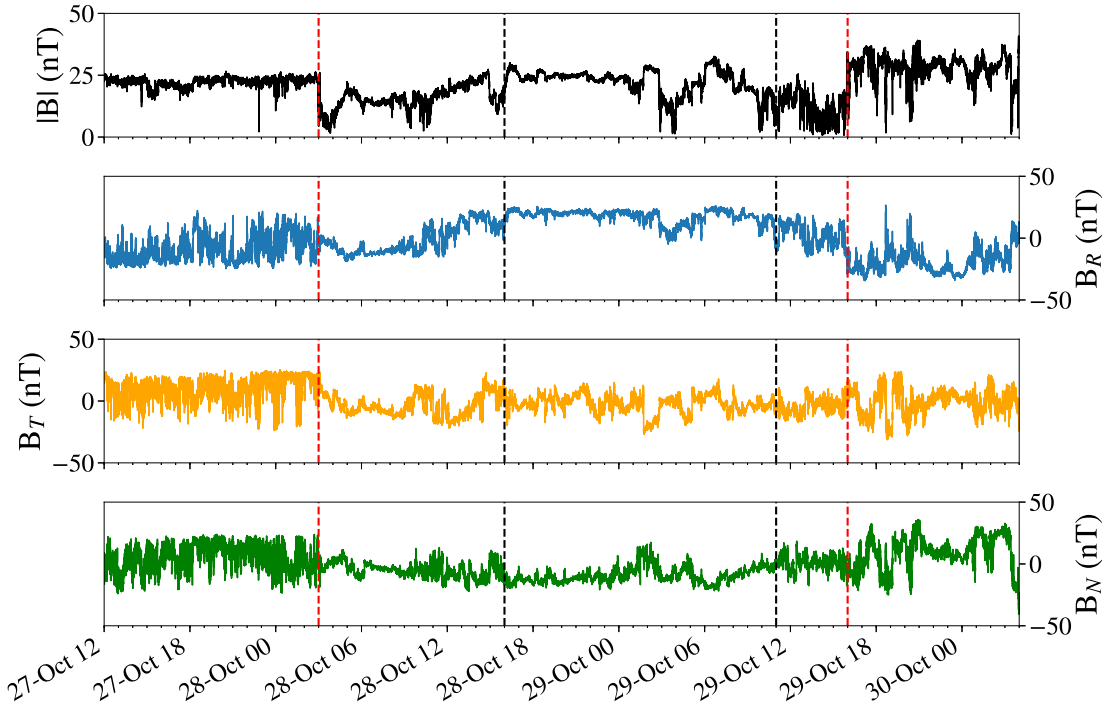

Figure 3.8: *Shows the magnetic field data for stream 1, lasting 37 hours on* 28^{th} *and* 29^{th} *October. The transition between negative and positive polarity is indicated by the first two dotted lines, taking 13 hours to make the switch. There is then a 19 hour period between the two black dotted lines where polarity is positive, followed by a 5 hour transition back to negative polarity. Also exhibits a weaker field magnitude inside the dotted red lines, indicating a higher thermal pressure.*

3.1.3 Magnetic Connectivity

A major advantage of the PFSS model is that it can be used to find the magnetic field line that connects Probe from the source surface to the solar surface, as detailed in Section 2.2.2. This is useful as the field line can then be plotted directly onto an image of the Sun, as demonstrated in Figure 3.9. Here the bottom axis represents the global structure of the corona, with the relevant part of the HCS plotted in white on the image above. Several magnetic field lines are shown connecting Probe to the two coronal holes in this image.

Such a process then allows for the realisation that Probe was connected to a small coronal hole from 31^{st} October to 14^{th} November. As discussed in the WSA model (Section 2.3.1), the size of the coronal hole influences the speed of the solar wind, so a slow wind prediction is still valid in this case. It is clear that stream 2 can also be classified as originating from a coronal hole, although the larger area means fast wind emanated from this region, as suggested by both the PFSS and MHD models.

This technique provides vital context for the magnetic field data, and can be considered a classification of solar wind type based on its origin which, crucially, was achieved without using any plasma data. This improves upon the predictions of solar wind as either slow or fast, which was described as simplistic in Section 1.2.2.

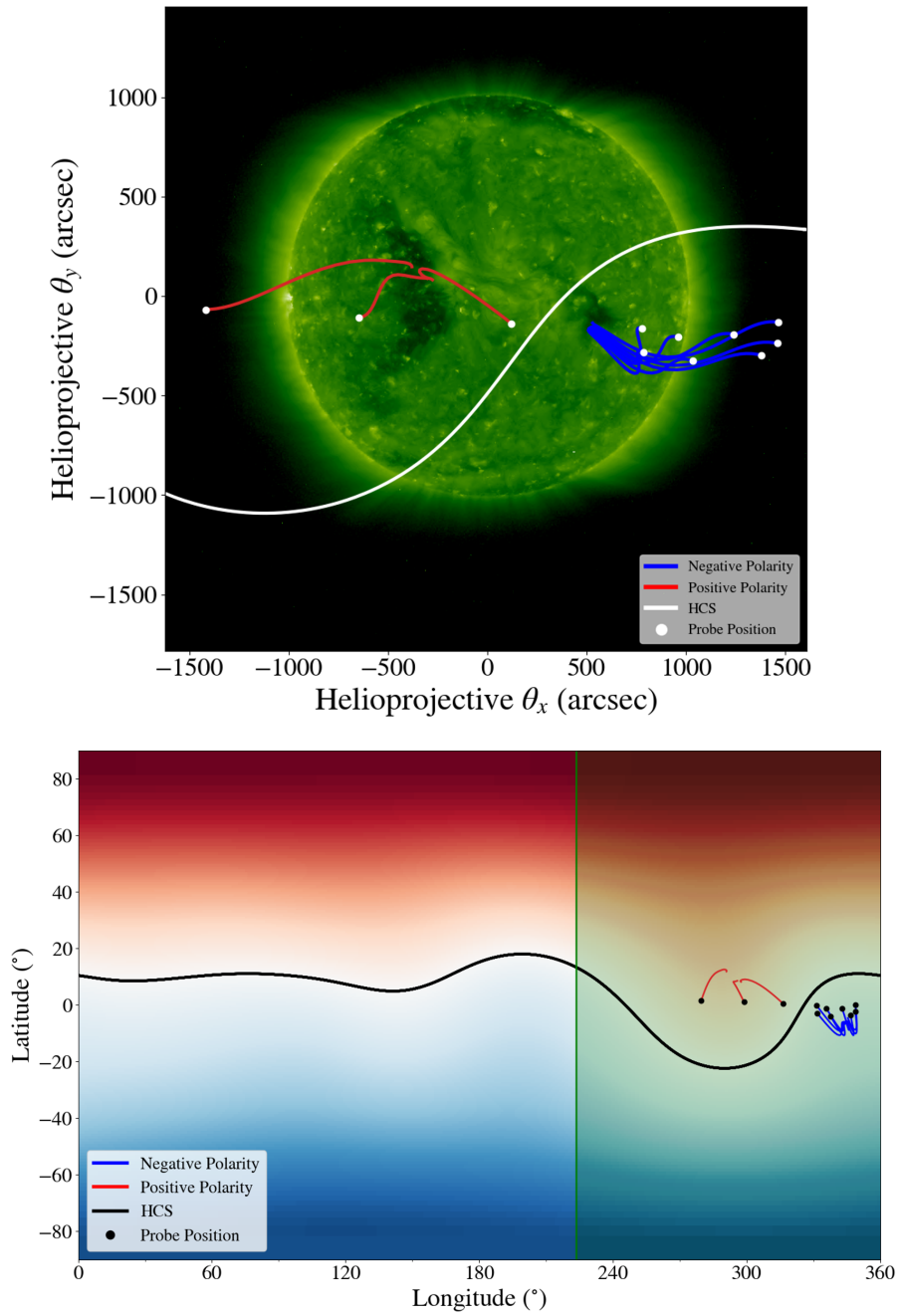

Figure 3.9: *Shows how the source region of the solar wind can be identified with the PFSS model and images of the Sun. The top image is from STEREO-A at a wavelength of* 195*Å on* 22^{nd} *October. The bottom axis shows the PFSS model using a magnetogram from* 6^{th} *November, with the HCS shown as the black line, and the field of view for the above image as the green highlight. Magnetic field lines every 2 days were integrated from Probe's position on the source surface, down to the solar surface, with the colour indicating the polarity. These and the HCS were then transformed into a helioprojective frame aligned with STEREO-A's position, and then plotted directly on the image. This demonstrates that Probe was connected to a small coronal hole at perihelion, and throughout stream 2 Probe was connected to a large coronal hole.*

3.2 Magnetic Footpoint Tracking

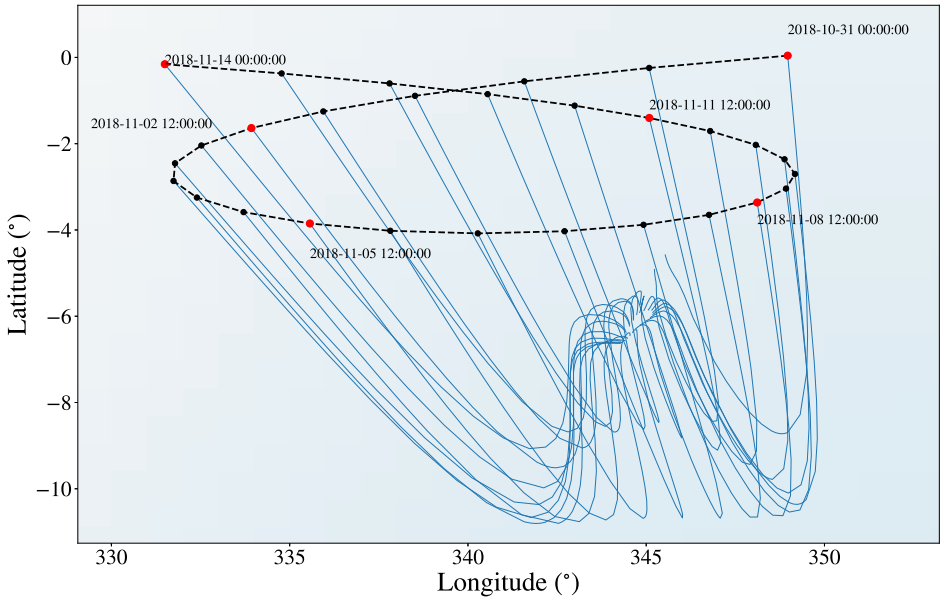

Figure 3.10: *Zoomed in map of Figure 3.9 at perihelion, with each dot representing Probe's position on the PFSS source surface 12 hours apart. Dates are shown for the red dots to help add context. Due to the coronal hole at perihelion, all the magnetic field lines connect to a similar region on the Sun's surface, creating a funnel shape.*

Figure 3.10 demonstrates that as a consequence of the coronal hole, all magnetic field lines connect to localised area on the Sun's surface. The reduced orbital speed of Probe in the Carrington frame is therefore magnified by the presence of this coronal hole.

The speed at which the magnetic footpoints track along on the Sun's surface is quantified in Figure 3.11, with the exceptionally low average footpoint speed of 130 ± 80km/h between 1^{st} and 14^{th} November. To put this in perspective, the Earth would track along the surface of the Sun at around 6400km/h. Speeds at this order of magnitude are indeed seen between 14^{th} and 23^{rd} November, indicating just how extraordinarily small the footpoint speed is around perihelion.

This represents an unprecedented view of spacecraft data, and could influence how much of the scientific research is carried out with Probe. Figure 3.11 displays how in situ measurements with Probe can represent solar wind originating from a particular point on the sun for hours at a time. It was anticipated by Fox et al. (2016, pg.18) that Probe's orbit alone would allow for a large range of temporal signatures to be seen. Crucially, it is the addition of the coronal hole at perihelion that has allowed the PFSS model to reveal unparalleled magnetic footpoint tracking speed.

It may be argued that the PFSS model is too simplistic, and there is an uncertainty of the footpoint speed presented in Figure 3.11. However, the exact values of the footpoint speed are essentially irrelevant, only the order of magnitude that they represent is of interest.

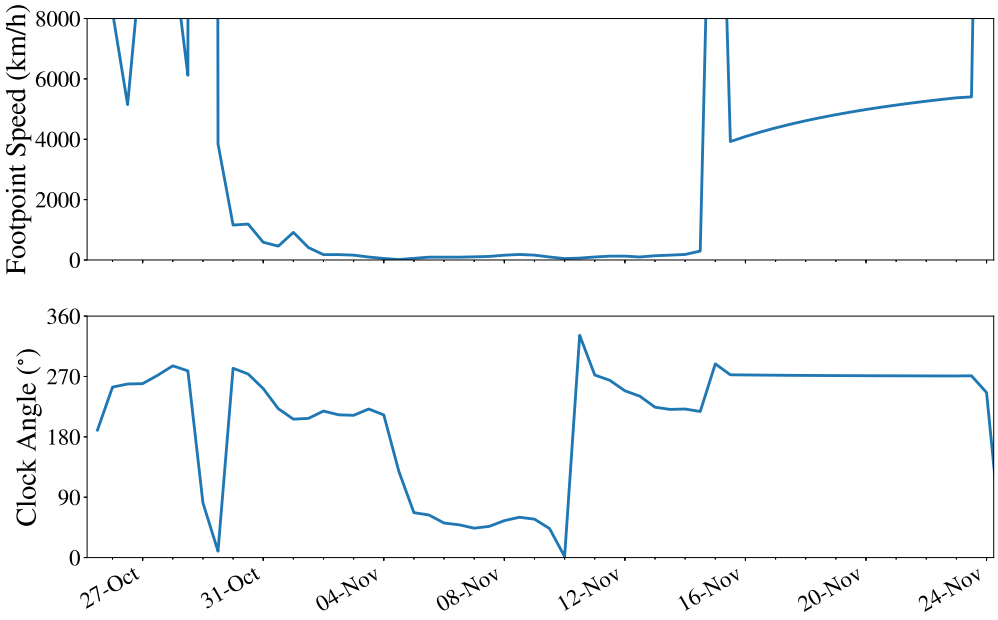

Figure 3.11: *The top axis shows how fast the magnetic footpoints track on the Sun's surface. This speed reduces to under* $200km/h$ *between* 1^{st} *and* 14^{th} *November, representing an order of magnitude difference than in the stream 2, between* 14^{th} *and* 23^{rd} *November. The bottom graph shows the clock angle, where* $0°$ *points directly up in latitude, and* $90°$ *points to higher Carrington longitude. Thus, there is a reversal in the direction of tracking between* 4^{th} *and* 5^{th} *November.*

3.2.1 Patchy/Quiet Regions

Probe's magnetic field data exhibited a feature never seen before by a spacecraft, that shall be referred to as 'patchy' and 'quiet' regions, as demonstrated in Figure 3.12. It is thought these new features are a consequence of the slow tracking speed in Figure 3.11, since all previous spacecraft travelled at great speed relative to the solar wind, unable to resolve small scale spatial and temporal features. The distinction between these two classifications is clear from the number of large amplitude peaks in the B_R component within a patchy region, compared to a quiet region. Since the fluctuations were present in the radial component, and the magnetic field magnitude within the peaks stays roughly constant, it was assumed that such fluctuations were Alfvénic in nature. Similar peaks have been identified at close distances with the Helios spacecraft (Matteini et al. 2014; Horbury, Matteini, and Stansby 2018), but there has never been a clear distinction between patchy/quiet regions. Perhaps this is due to such regions blending together as they propagate outwards, or the footpoint tracking speed being too high to distinguish between them. These two effects are most likely combining, since slow tracking speeds in Figure 3.11 are only present when the distance to the Sun is low.

The patches themselves were identified using visual inspection, however, an algorithm was used to identify the peaks. This was achieved by smoothing B_R over 2 hours with a boxcar average ($\langle B_R \rangle$), and the field magnitude over 10 hours ($\langle |B| \rangle$) so that a background value was obtained.

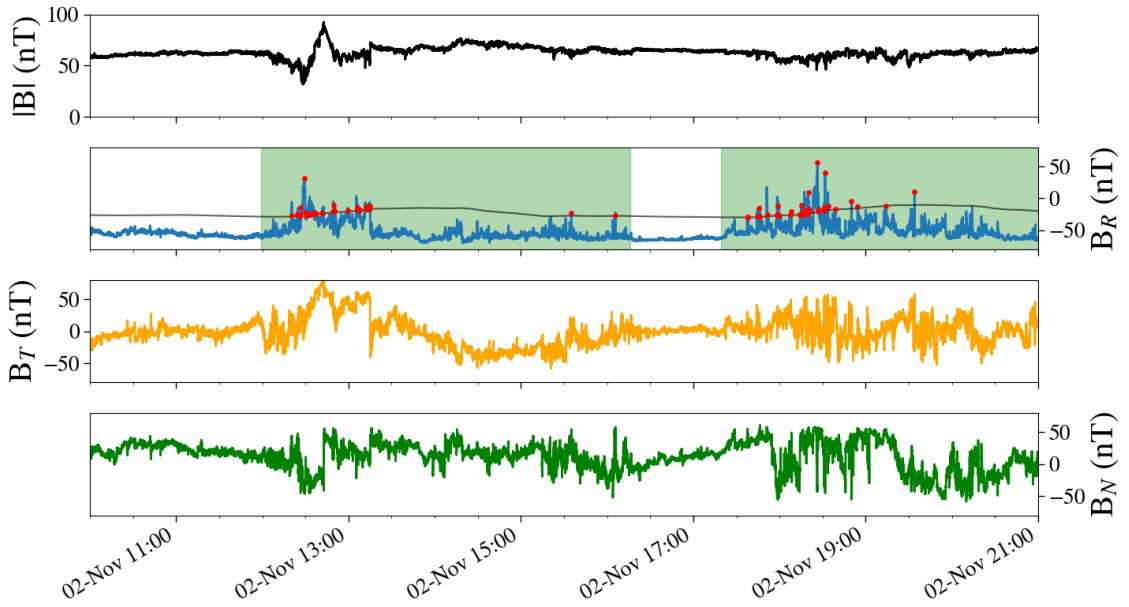

Figure 3.12: *Demonstrates patchy (green highlight) and quiet regions in the magnetic field data, identified by eye. The peaks identified are shown by a red scatter point, and the threshold* $\frac{1}{2}\langle|B|\rangle$ *above the background* B_R *is shown as the smooth black line on the* B_R *axis. (Credit: Project Partner)*

A peak was therefore defined according to the following condition:

$$B_R - \langle B_R \rangle > \frac{1}{2}\langle|B|\rangle\,. \tag{3.1}$$

In order to estimate a length scale of such regions on the surface of the Sun, their duration was multiplied by the average footpoint speed from Figure 3.11. The results of this and the peaks statistics are shown in Table 3.1. The most striking feature of these results is that they are mere hundreds of km on the Sun's surface, where the Sun has a circumference of 4.4 million km.

	Total No	Avg Duration	Waiting Time	Length Scale
Spikes	6752	10-50s	2-5mins	-
Patchy Regions	25	5hrs 11mins	-	∼600km
Quiet Regions	19	2hr 2 mins	-	∼200km

Table 3.1: *Summary of the statistics regarding the patchy and quiet regions, along with the peaks identified. All of these regions were identified between the* 1^{st} *and* 14^{th} *November, where the footpoint speed is low as in Figure 3.11. The spikes represent 9.1% of a patchy region, which is larger than the 5% reported by Horbury et al. (2018). (Credit: Project Partner).*

[Edit: removed this section]

3.2.2 Possible Explanations

The magnitude of the magnetic field is seen to reduce within a patchy region, with many fluctuations compared to the steady field in a quiet region, as seen in Figure 3.12. This suggests that the plasma properties between the two regions may be different, with a higher thermal pressure in the patchy region. It will be interesting to determine if such regions are fundamentally different in their composition and properties, although this requires data from the other instrument suites on Probe.

The length scales presented in Table 3.1 match within an order of magnitude to the size of granules of the photosphere, which have a scale $\sim$ 1300km and a lifetime of 8-20 minutes (Javaherian et al. 2014). This means that Probe could be connected to a single granule for longer than its lifetime, which has never happened before. One possible explanation for the patchy regions is that these originate from the photospheric bright points, that sit in the inter granular lanes as mentioned in Section 1.1. It is proposed that magnetic reconnection within these photospheric bright points launches jets of particles and Alfvén waves into the corona. Magnetic reconnection driven by granular motion has been observed by Zeng et al. (2013). Therefore, patchy regions correspond to times where Probe is connected to the edge of a granule, whereas a quiet region originates from the centre of a granule where there is little activity. Such a theory is consistent with the scale lengths, as the magnetic field lines from a granule edge are more expanded than those lines from the centre of a granule, corresponding to a larger length scale for the patchy regions.

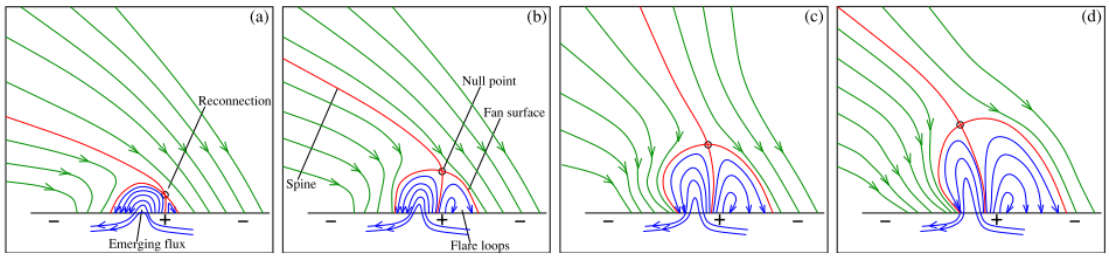

Figure 3.13: *Diagram for a proposed theory for the formation of a coronal hole jet over time, due to reconnection between open (green) and closed (blue) field lines. This creates a jet along the red spine, whose orientation changes from (a) to (d), that is described as a whip-like motion. (Credit: Liu et al. (2011)).*

Zeng et al. (2016) state that jets observed with telescopes tend to recur from the same region, perhaps being part of a longer process of reconnection. There have also been suggestions that such jets have a well defined structure, as shown in Figure 3.13, and can even present a whip-like motion changing the orientation of the jet over time (Liu et al. 2011). So perhaps each peak within a patch originates from the same process of magnetic reconnection. Although their origin is still open to debate, it is clear that there is some underlying repeatable process responsible.

With the evidence presented in this report, it is believed that particle jets are launched by magnetic reconnection at a localised region on the Sun, manifesting as a patchy region. These then blend into the background solar wind flow represented by the quiet regions, therefore accelerating the solar wind. This also explains why the patchy/quiet regions are a new discovery for Probe, as the distinction between them would not possible if they merged at larger distances from the Sun.

Chapter 4

Conclusion

Predictions for solar wind conditions to be experienced by Probe were first made with an MHD model, that proved to be accurate in velocity, temperature and density. This was evaluated against data from the ACE satellite, since only magnetic field data was accessible from Probe. Such a successful prediction achieved one of the initial aims of the project, with the principal investigator of the FIELDS instrument being made aware of this work.

However, it was clear that the MHD model lacked the ability to properly model the magnetic field of the solar wind, and equally could not react quickly enough to changes to the coronal magnetic field. Therefore, the PFSS model was then implemented with a ballistic mapping technique to provide more accurate and up to date models of the coronal magnetic field. It was shown that such a method was accurate in predicting the polarity of the magnetic field throughout the first perihelion, and was used to explain the non-trivial origin of the small positive polarity stream between 28^{th} and 29^{th} October 2018.

For future orbits, Probe will sample the solar wind below the inner boundary of the computationally expensive Enlil part of the MHD model, meaning it will be obsolete for this mission. Therefore, it will be important to create an open source implementation of the WSA model to allow for the determination of important solar wind parameters not offered by the PFSS model.

However, this drawback of the PFSS model was more than compensated for by the use of STEREO-A images to provide classification of the solar wind type by linking to coronal holes on the Sun. This again showed the PFSS model was versatile in its application, and allowed for the classification of solar wind type to be made without any plasma data.

The unique orbit of Probe was recognised as something that could be exploited and investigated as part of this project. The speed in the Sun's rotating frame was already anticipated to allow for Probe to study regions on the Sun over prolonged periods. However, it was through the PFSS model that a small coronal hole at perihelion was identified, highlighting how all magnetic field lines around this section of the orbit connected to a very localised region on the Sun's surface. Analysis of the speed at which these magnetic footpoints tracked along the surface, led to the surprising result that the average speed was 130 ± 80km/h over a two week period. It was thought that such a striking result could change the way researchers view data from Probe, as all previous spacecraft flew at great speeds relative to the solar wind. This goes well beyond the initial aim of the project, as it depended on the

fortunate appearance of a coronal hole at perihelion.

This also provided some insight into the never before seen patchy and quiet regions in the magnetic field data. Statistics on the duration of these regions were paired with estimated footpoint speed to evaluate the length scales as hundreds of km on the surface of the Sun. This appeared to match the length scales of granules on the photosphere, leading to the idea of jets launched from magnetic reconnection at the granule boundaries. Matching Probe's in situ data with telescope observations of jets, such as those from the Hinode spacecraft, will be crucial to understanding their origin.

The inclusion of plasma data will be essential to understand the process that created these coherent structures. This will also allow for the estimation of the peak's momentum and energy, in order to evaluate their role in accelerating the solar wind, a long outstanding question in space physics that Probe aims to solve.

Acknowledgements

I have received a great deal of support throughout this project. I would firstly like to thank my supervisor, Prof. Tim Horbury, for allowing my project partner and I to participate in the Parker Solar Probe mission, especially for presenting our work to the FIELDS team. You have made this project exciting and for that I'm very grateful.

I would to extend a massive thank you to David Stansby for writing the `PfssPy` and `HelioPy` packages that were invaluable to this research, and for helping me several times along the way. I would also like to thank Dr. Denise Perrone for attending our weekly meetings throughout this project, and pointing me in the direction of key papers to aid my understanding.

I am particularly grateful for the support of Olivia Williams, whom I'm assured now knows everything about the solar wind, despite dropping physics after GCSE. Thanks to my project partner for the many useful discussions and thank you to Philip Moloney for your advice.

Finally, I would like to thank my parents for their continued support.

Bibliography

Abbo, L., L. Ofman, S. K. Antiochos, V. H. Hansteen, L. Harra, Y.-K. Ko, G. Lapenta, B. Li, P. Riley, L. Strachan, R. von Steiger, and Y.-M. Wang (2016). "Slow Solar Wind: Observations and Modeling". In: *Space Science Reviews* 201.1-4, pp. 55–108. ISSN: 0038-6308. DOI: 10.1007/s11214-016-0264-1.

Acton, Charles H. (1996). "Ancillary data services of NASA's Navigation and Ancillary Information Facility". In: *Planetary and Space Science* 44.1, pp. 65–70. DOI: 10.1016/0032-0633(95)00107-7.

Acton, Charles, Nathaniel Bachman, Boris Semenov, and Edward Wright (2018). "A look towards the future in the handling of space science mission geometry". In: *Planetary and Space Science* 150, pp. 9–12. ISSN: 00320633. DOI: 10.1016/j.pss.2017.02.013.

Alfvén, Hannes (1942). "Existence of Electromagnetic-Hydrodynamic Waves". In: *Nature* 150.3805, pp. 405–406. ISSN: 0028-0836. DOI: 10.1038/150405d0.

— (1977). "Electric currents in cosmic plasmas". In: *Reviews of Geophysics* 15.3, pp. 271–284. ISSN: 19449208. DOI: 10.1029/RG015i003p00271.

Altschuler, Martin D. and Gordon Newkirk (1969). "Magnetic fields and the structure of the solar corona". In: *Solar Physics* 9.1, pp. 131–149. ISSN: 0038-0938. DOI: 10.1007/BF00145734.

Annex, Andrew, Brian Carcich, kd7uiy, The Gitter Badger, Shin-ya Murakami, Shankar Kulumani, Miguel de Val-Borro, Marcel Stefko, Jorge Diaz del Rio, and B. Seignovert (2019). "AndrewAnnex/SpiceyPy: SpiceyPy 2.2.0". In: DOI: 10.5281/ZENODO.2576445.

Arden, W. M., A. A. Norton, and X. Sun (2014). "A "breathing" source surface for cycles 23 and 24". In: *Journal of Geophysical Research: Space Physics* 119.3, pp. 1476–1485. ISSN: 21699380. DOI: 10.1002/2013JA019464.

Arge, C. N. and V. J. Pizzo (2000). "Improvement in the prediction of solar wind conditions using near-real time solar magnetic field updates". In: *Journal of Geophysical Research: Space Physics* 105.A5, pp. 10465–10479. ISSN: 01480227. DOI: 10.1029/1999JA000262.

Arge, C.N., J.G. Luhmann, D. Odstrcil, C.J. Schrijver, and Y. Li (2004). "Stream structure and coronal sources of the solar wind during the May 12th, 1997 CME". In: *Journal of Atmospheric and Solar-Terrestrial Physics* 66, pp. 1295–1309. ISSN: 1364-6826. DOI: 10.1016/J.JASTP.2004.03.018.

Arlt, R. (2011). "The sunspot observations by Samuel Heinrich Schwabe". In: *Astronomische Nachrichten* 332.8, pp. 805–814. ISSN: 00046337. DOI: 10.1002/asna.201111601.

Bale, S. D. et al. (2016). "The FIELDS Instrument Suite for Solar Probe Plus: Measuring the Coronal Plasma and Magnetic Field, Plasma Waves and Turbu-

lence, and Radio Signatures of Solar Transients". In: *Space Science Reviews* 204, pp. 49–82. ISSN: 15729672. DOI: 10.1007/s11214-016-0244-5.

Biermann, L. (1957). "Solar corpuscular radiation and the interplanetary gas". In: *The Observatory* 77, pp. 109–110. URL: http://adsabs.harvard.edu/abs/1957Obs....77..109B.

Biskamp, D. (2000). *Magnetic reconnection in plasmas*. Cambridge University Press. ISBN: 0521582881.

Bochsler, P (2007). "Minor ions in the solar wind". In: *Astron Astrophys Rev* 14, pp. 1–40. DOI: 10.1007/s00159-006-0002-x.

Camporeale, Enrico, Algo Carè, and Joseph E Borovsky (2017). "Classification of Solar Wind With Machine Learning". In: *Journal of Geophysical Research: Space Physics* 122.11, pp. 910–10. DOI: 10.1002/2017JA024383.

Carrington, R. C. (1853). *Observations of the spots on the sun from November 9, 1853, to March 24, 1861, made at Redhill*. URL: https://archive.org/details/observationsofsp00carr/page/n4.

Charbonneau, Paul (2010). "Dynamo Models of the Solar Cycle". In: *Living Reviews in Solar Physics* 7.1, p. 3. DOI: 10.12942/lrsp-2010-3.

Cornish, Neil (2019). *What is a Lagrange Point?* URL: https://solarsystem.nasa.gov/resources/754/what-is-a-lagrange-point/.

Cranmer, Steven R. (2009). "Coronal Holes". In: *Living Reviews in Solar Physics* 6.1, p. 3. ISSN: 1614-4961. DOI: 10.12942/lrsp-2009-3.

Cranmer, Steven R. and Amy R. Winebarger (2018). "The Properties of the Solar Corona and Its Connection to the Solar Wind". In: URL: http://arxiv.org/abs/1811.00461.

Crooker, N U, Chia-Lin L Huang, S M Lamassa, D E Larson, S W Kahler, and H E Spence (2004). "Heliospheric Plasma Sheets". In: *J. Geophys. Res* 109, p. 3107. DOI: 10.1029/2003JA010170.

D'Amicis, R. and R. Bruno (2015). "ON THE ORIGIN OF HIGHLY ALFVÉNIC SLOW SOLAR WIND". In: *The Astrophysical Journal* 805.1, p. 84. ISSN: 1538-4357. DOI: 10.1088/0004-637X/805/1/84.

De Pontieu, Bart, Scott W. McIntosh, Viggo H. Hansteen, and Carolus J. Schrijver (2009). "OBSERVING THE ROOTS OF SOLAR CORONAL HEATING—IN THE CHROMOSPHERE". In: *The Astrophysical Journal* 701.1, pp. L1–L6. ISSN: 0004-637X. DOI: 10.1088/0004-637X/701/1/L1.

Domingo, V., B. Fleck, and A. I. Poland (1995). "SOHO: The Solar and Heliospheric Observatory". In: *Space Science Reviews* 72.1-2, pp. 81–84. ISSN: 0038-6308. DOI: 10.1007/BF00768758.

Driel-Gesztelyi, Lidia van and Lucie May Green (2015). "Evolution of Active Regions". In: *Living Reviews in Solar Physics* 12.1, p. 1. ISSN: 2367-3648. DOI: 10.1007/lrsp-2015-1.

Dunbar, B (2012). *Layers of the Sun*. URL: https://www.nasa.gov/mission_pages/iris/multimedia/layerzoo.html.

Eastwood, J. P., R. Nakamura, L. Turc, L. Mejnertsen, and M. Hesse (2017). "The Scientific Foundations of Forecasting Magnetospheric Space Weather". In: *Space Science Reviews* 212.3-4, pp. 1221–1252. ISSN: 0038-6308. DOI: 10.1007/s11214-017-0399-8.

Edwards, S J, A R Yeates, F.-X Bocquet, and D H Mackay (2015). *Influence of Non-Potential Coronal Magnetic Topology on Solar-Wind Models*. Tech. rep. URL: https://arxiv.org/pdf/1511.00427.pdf.

ESA (2019). *How many stars are there in the Universe?* URL: https://www.esa.int/Our_Activities/Space_Science/Herschel/How_many_stars_are_there_in_the_Universe.

Fox, N. J., M. C. Velli, S. D. Bale, R. Decker, A. Driesman, R. A. Howard, J. C. Kasper, J. Kinnison, M. Kusterer, D. Lario, M. K. Lockwood, D. J. McComas, N. E. Raouafi, and A. Szabo (2016). "The Solar Probe Plus Mission: Humanity's First Visit to Our Star". In: *Space Science Reviews*, pp. 7–48. ISSN: 15729672. DOI: 10.1007/s11214-015-0211-6.

Fränz, M and D Harper (2002). *Heliospheric Coordinate Systems*. Tech. rep. URL: http://www.nao.rl.ac.uk/.

Georgoulis, Manolis K., Marco Velli, and Giorgio Einaudi (1998). "Statistical Properties of Magnetic Activity in the Solar Corona". In: *The Astrophysical Journal* 497.2, pp. 957–966. ISSN: 0004-637X. DOI: 10.1086/305486.

Gringauz, K. I., V. V. Bezrokikh, V. D. Ozerov, and R. E. Rybchinskii (1960). "A Study of the Interplanetary Ionized Gas, High-Energy Electrons and Corpuscular Radiation from the Sun by Means of the Three-Electrode Trap for Charged Particles on the Second Soviet Cosmic Rocket". In: *Soviet Physics Doklady* 5, p. 361. URL: http://adsabs.harvard.edu/abs/1960SPhD....5..361G.

Habbal, S R, R Woo, S Fineschi, R O'neal, J Kohl, G Noci, and C Korendyke (1997). *ORIGINS OF THE SLOW AND THE UBIQUITOUS FAST SOLAR WIND*. Tech. rep., pp. 103–106. URL: http://iopscience.iop.org/article/10.1086/310970/pdf.

Henriques, Vasco (2010). *High Resolution Granulation*. URL: https://www.isf.astro.su.se/.

Hill, Frank, George Fischer, Jennifer Grier, John W. Leibacher, Harrison B. Jones, Patricia P. Jones, Renate Kupke, and Robin T. Stebbins (1994). "The global oscillation network group site survey 1: Data collection and analysis methods". In: *Solar Physics* 152.2, pp. 321–349. DOI: 10.1007/BF00680443.

Hindmarsh, Alan (1983). "ODEPACK, A Systematized Collection of ODE Solvers". In: *IMACS Transactions on Scientific Computation* 1, pp. 55–64. URL: https://www3.nd.edu/~powers/ame.60636/hindmarsh1983.pdf.

Hoeksema, J. Todd, John M. Wilcox, and Philip H. Scherrer (1983). "The structure of the heliospheric current sheet: 1978–1982". In: *Journal of Geophysical Research* 88.A12, p. 9910. ISSN: 0148-0227. DOI: 10.1029/JA088iA12p09910.

Horbury, T S, L Matteini, and D Stansby (2018). "Short, large-amplitude speed enhancements in the near-Sunfast solar wind". In: *Monthly Notices of the Royal Astronomical Society* 478.2, pp. 1980–1986. ISSN: 0035-8711. DOI: 10.1093/mnras/sty953.

Hospodarsky, George B. (2016). "Spaced-based search coil magnetometers". In: *Journal of Geophysical Research: Space Physics* 121.12, pp. 068–12. ISSN: 21699380. DOI: 10.1002/2016JA022565.

Howard, R. A. et al. (2008). "Sun Earth Connection Coronal and Heliospheric Investigation (SECCHI)". In: *Space Science Reviews* 136.1-4, pp. 67–115. ISSN: 0038-6308. DOI: 10.1007/s11214-008-9341-4.

Isenberg, Philip A. (2001). "Heating of Coronal Holes and Generation of the Solar Wind by Ion-Cyclotron Resonance". In: *Space Science Reviews* 95.1/2, pp. 119–131. ISSN: 00386308. DOI: 10.1023/A:1005287225222.

Ivory, Kevin (1999). *Helios*. URL: https://www2.mps.mpg.de/en/projekte/helios/#e2.

Javaherian, M., H. Safari, A. Amiri, and S. Ziaei (2014). "Automatic Method for Identifying Photospheric Bright Points and Granules Observed by Sunrise". In: *Solar Physics* 289.10, pp. 3969–3983. ISSN: 0038-0938. DOI: 10.1007/s11207-014-0555-1.

Jian, L. K., P. J. MacNeice, A. Taktakishvili, D. Odstrcil, B. Jackson, H.-S. Yu, P. Riley, I. V. Sokolov, and R. M. Evans (2015). "Validation for solar wind prediction at Earth: Comparison of coronal and heliospheric models installed at the CCMC". In: *Space Weather* 13.5, pp. 316–338. ISSN: 15427390. DOI: 10.1002/2015SW001174.

Jian, L. K., C. T. Russell, J. G. Luhmann, P. J. MacNeice, D. Odstrcil, P. Riley, J. A. Linker, R. M. Skoug, and J. T. Steinberg (2011). "Comparison of Observations at ACE and Ulysses with Enlil Model Results: Stream Interaction Regions During Carrington Rotations 2016 – 2018". In: *Solar Physics* 273.1, pp. 179–203. ISSN: 0038-0938. DOI: 10.1007/s11207-011-9858-7.

Jones, E, E Oliphant, P Peterson, et al. (2019). *SciPy: Open Source Scientific Tools for Python*. URL: http://www.scipy.org/.

Kasper, J. C., A. J. Lazarus, and S. P. Gary (2008). "Hot Solar-Wind Helium: Direct Evidence for Local Heating by Alfvén-Cyclotron Dissipation". In: *Physical Review Letters* 101.26, p. 261103. ISSN: 0031-9007. DOI: 10.1103/PhysRevLett.101.261103.

Kasper, Justin C., Robert Abiad, et al. (2016). "Solar Wind Electrons Alphas and Protons (SWEAP) Investigation: Design of the Solar Wind and Coronal Plasma Instrument Suite for Solar Probe Plus". In: *Space Science Reviews* 204, pp. 131–186. ISSN: 15729672. DOI: 10.1007/s11214-015-0206-3.

Keys, P H, M Mathioudakis, D B Jess, S Shelyag, D J Christian, and F P Keenan (2013). "Tracking magnetic bright point motions through the solar atmosphere". In: *MNRAS* 428, pp. 3220–3226. DOI: 10.1093/mnras/sts268.

Kuperus, Max, James A. Ionson, and Daniel S. Spicer (1981). "On the Theory of Coronal Heating Mechanisms". In: *Annual Review of Astronomy and Astrophysics* 19.1, pp. 7–40. ISSN: 0066-4146. DOI: 10.1146/annurev.aa.19.090181.000255.

Lasley, Scott (2016). *Carrington Rotation Number*. URL: http://umtof.umd.edu/pm/crn/.

Liu, Wei, Thomas E Berger, Alan M Title, Theodore D Tarbell, and B C Low (2011). "CHROMOSPHERIC JET AND GROWING LOOP OBSERVED BY HINODE: NEW EVIDENCE OF FAN-SPINE MAGNETIC TOPOLOGY RESULTING FROM FLUX EMERGENCE". In: *The Astrophysical Journal* 728.16pp, p. 103. DOI: 10.1088/0004-637X/728/2/103.

Mackay, Duncan and Anthony Yeates (2012). "The Sun's Global Photospheric and Coronal Magnetic Fields: Observations and Models". In: *Living Reviews in Solar Physics* 9.1, p. 6. ISSN: 1614-4961. DOI: 10.12942/lrsp-2012-6.

Malaspina, David M., Robert E. Ergun, Mary Bolton, Mark Kien, David Summers, Ken Stevens, Alan Yehle, Magnus Karlsson, Vaughn C. Hoxie, Stuart D. Bale,

and Keith Goetz (2016). "The Digital Fields Board for the FIELDS instrument suite on the Solar Probe Plus mission: Analog and digital signal processing". In: *Journal of Geophysical Research: Space Physics* 121.6, pp. 5088–5096. ISSN: 21699380. DOI: 10.1002/2016JA022344.

Matteini, Lorenzo, Timothy S. Horbury, Marcia Neugebauer, and Bruce E. Goldstein (2014). "Dependence of solar wind speed on the local magnetic field orientation: Role of Alfvénic fluctuations". In: *Geophysical Research Letters* 41.2, pp. 259–265. ISSN: 00948276. DOI: 10.1002/2013GL058482.

McComas, D. J., H. A. Elliott, N. A. Schwadron, J. T. Gosling, R. M. Skoug, and B. E. Goldstein (2003). "The three-dimensional solar wind around solar maximum". In: *Geophysical Research Letters* 30.10. ISSN: 00948276. DOI: 10.1029/2003GL017136.

McComas, D J, P Riley, J T Gosling, A. Balogh, and R. Forsyth (1998). "Ulysses' rapid crossing of the polar coronal hole boundary". In: *Journal of Geophysical Research*. ISSN: 0148-0227. DOI: 10.1029/97JA01459.

McComas, D J, M Velli, et al. (2007). "Understanding coronal heating and solar wind acceleration: Case for in situ near-Sun measurements". In: *Reviews of Geophysics* 45. DOI: 10.1029/2006RG000195.

Miles, David M., Ian R. Mann, Andy Kale, David K. Milling, Barry B. Narod, John R. Bennest, David Barona, and Martyn J. Unsworth (2017). "The effect of winding and core support material on the thermal gain dependence of a fluxgate magnetometer sensor". In: *Geoscientific Instrumentation, Methods and Data Systems* 6.2, pp. 377–396. ISSN: 2193-0864. DOI: 10.5194/gi-6-377-2017.

Mumford, Stuart et al. (2019). "sunpy/sunpy: v0.9.6". In: DOI: 10.5281/ZENODO.2551710.

NASA/SDO (2015). *Coronal Hole Front and Center*. URL: https://www.nasa.gov/image-feature/goddard/coronal-hole-front-and-center.

Ness, N. F. (1970). "Magnetometers for space research". In: *Space Science Reviews* 11.4, pp. 459–554. DOI: 10.1007/BF00183028.

Neugebauer, M., P. C. Liewer, E. J Smith, R. M. Skoug, and T. H. Zurbuchen (2002). "Sources of the solar wind at solar activity maximum". In: *Journal of Geophysical Research: Space Physics* 107.A12, pp. 13–1. ISSN: 01480227. DOI: 10.1029/2001JA000306.

Neugebauer, Marcia and Conway W. Snyder (1966). "Mariner 2 observations of the solar wind: 1. Average properties". In: *Journal of Geophysical Research* 71.19, pp. 4469–4484. ISSN: 01480227. DOI: 10.1029/JZ071i019p04469.

Noci, G (2002). "The Temperature of the Solar Corona". In: *Mem. S.A.It* 74, p. 704. URL: http://sait.oat.ts.astro.it/MmSAI/74/PDF/704.pdf.

Odstrcil, D. (2003). "Modeling 3-D solar wind structure". In: *Advances in Space Research* 32.4, pp. 497–506. ISSN: 0273-1177. DOI: 10.1016/S0273-1177(03)00332-6.

Ogilvie, Keith W. and George K. Parks (1996). "First results from WIND spacecraft: An introduction". In: *Geophysical Research Letters* 23.10, pp. 1179–1181. ISSN: 00948276. DOI: 10.1029/96GL01357.

Owens, M. J., H. E. Spence, S. McGregor, W. J. Hughes, J. M. Quinn, C. N. Arge, P. Riley, J. Linker, and D. Odstrcil (2008). "Metrics for solar wind prediction models: Comparison of empirical, hybrid, and physics-based schemes

with 8 years of L1 observations". In: *Space Weather* 6. ISSN: 15427390. DOI: 10.1029/2007SW000380.

Parker, E. N. (1958a). "Cosmic-Ray Modulation by Solar Wind". In: *Physical Review* 110.6, pp. 1445–1449. ISSN: 0031-899X. DOI: 10.1103/PhysRev.110.1445.

— (1958b). "Dynamics of the Interplanetary Gas and Magnetic Fields". In: *The Astrophysical Journal* 128, p. 664. ISSN: 0004-637X. DOI: 10.1086/146579.

— (1988). "Nanoflares and the solar X-ray corona". In: *The Astrophysical Journal* 330, pp. 474–479. DOI: 10.1086/166485.

— (2001). "A history of the Solar Wind concept". In: *The Century of Space Science*. Ed. by J.A.M. Bleeker, J. Geiss, and M.C.E. Huber. Springer Netherlands, pp. 225–255. ISBN: 978-0-7923-7196-0. DOI: 10.1007/978-94-010-0320-9.

Petzold, Linda (1983). "Automatic Selection of Methods for Solving Stiff and Nonstiff Systems of Ordinary Differential Equations". In: *SIAM Journal on Scientific and Statistical Computing* 4.1, pp. 136–148. ISSN: 0196-5204. DOI: 10.1137/0904010.

Pizzo, Vic, George Millward, Annette Parsons, Douglas Biesecker, Steve Hill, and Dusan Odstrcil (2011). "Wang-Sheeley-Arge-Enlil cone model transitions to operations". In: *Space Weather* 9.3. ISSN: 15427390. DOI: 10.1029/2011SW000663.

Porsche, H. (1977). "General aspects of the mission Helios 1 and 2. Introduction to a special issue on initial scientific results of the Helios Mission." In: *Journal of Geophysics* 42, pp. 551–559. URL: http://adsabs.harvard.edu/abs/1977JGZG...42..551P.

Priest, E. R. (Eric Ronald), Terry Forbes, and Cambridge University Press. (2000). *Magnetic reconnection : MHD theory and applications*. Cambridge University Press. ISBN: 9780511525087. DOI: 10.1017/CBO9780511525087.

Reiss, Martin A., Peter J. MacNeice, Leila M. Mays, Charles N. Arge, Christian Möstl, Ljubomir Nikolic, and Tanja Amerstorfer (2019). "Forecasting the Ambient Solar Wind with Numerical Models. I. On the Implementation of an Operational Framework". In: *The Astrophysical Journal Supplement Series* 240.2, p. 35. ISSN: 1538-4365. DOI: 10.3847/1538-4365/aaf8b3.

Riley, Pete, J. A. Linker, Z. Mikić, R. Lionello, S. A. Ledvina, and J. G. Luhmann (2006). "A Comparison between Global Solar Magnetohydrodynamic and Potential Field Source Surface Model Results". In: *The Astrophysical Journal* 653.2, pp. 1510–1516. ISSN: 0004-637X. DOI: 10.1086/508565.

Rosenberg, Ronald L. and Paul J. Coleman (1969). "Heliographic latitude dependence of the dominant polarity of the interplanetary magnetic field". In: *Journal of Geophysical Research* 74.24, pp. 5611–5622. ISSN: 01480227. DOI: 10.1029/JA074i024p05611.

Rouillard, A. P., J. A. Davies, B. Lavraud, R. J. Forsyth, N. P. Savani, D. Bewsher, D. S. Brown, N. R. Sheeley, C. J. Davis, R. A. Harrison, R. A. Howard, A. Vourlidas, M. Lockwood, S. R. Crothers, and C. J. Eyles (2010). "Intermittent release of transients in the slow solar wind: 1. Remote sensing observations". In: *Journal of Geophysical Research: Space Physics* 115.A4103. ISSN: 01480227. DOI: 10.1029/2009JA014471.

Schatten, Kenneth H. (1972). "Current Sheet Magnetic Model for the Solar Corona". In: *Solar Wind. Edited by Charles P. Sonett, Paul J. Coleman, and John M. Wilcox. Washington, Scientific and Technical Information Office, National Aeronautics and Space Administration., p.44* 308, p. 44.

Schatten, Kenneth H., John M. Wilcox, and Norman F. Ness (1969). "A model of interplanetary and coronal magnetic fields". In: *Solar Physics* 6.3, pp. 442–455. ISSN: 0038-0938. DOI: 10.1007/BF00146478.

Schwadron, N. A., D. J. McComas, H. A. Elliott, G. Gloeckler, J. Geiss, and R. von Steiger (2005). "Solar wind from the coronal hole boundaries". In: *Journal of Geophysical Research: Space Physics* 110.A4. ISSN: 01480227. DOI: 10.1029/2004JA010896.

Schwenn, R. (1983). "The average solar wind in the inner heliosphere: Structures and slow variations". In: *JPL Solar Wind Five*, pp. 489–507. URL: https://ntrs.nasa.gov/archive/nasa/casi.ntrs.nasa.gov/19840005037.pdf.

Schwenn, R and E Marsch (1990). *Physics of the Inner Heliosphere I*. Ed. by M.C.E. Huber, L.J. Lanzerotti, and D Stoffler. Vol. 1. ISBN: 978-3-642-75363-3. DOI: 10.1007/978-3-642-75361-9.

Sheeley Jr, Neil R (2017). "Origin of the Wang-Sheeley-Arge solar wind model". In: *Hist. Geo Space Sci* 8, pp. 21–28. DOI: 10.5194/hgss-8-21-2017.

Sheeley, N. R., J. W. Harvey, and W. C. Feldman (1976). "Coronal holes, solar wind streams, and recurrent geomagnetic disturbances: 1973-1976". In: *Solar Physics* 49.2, pp. 271–278. ISSN: 0038-0938. DOI: 10.1007/BF00162451.

Smith, Edward J. (2001). "The heliospheric current sheet". In: *Journal of Geophysical Research: Space Physics* 106.A8, pp. 15819–15831. ISSN: 01480227. DOI: 10.1029/2000JA000120.

Stansby, D., T. S. Horbury, and L. Matteini (2019). "Diagnosing solar wind origins using in-situ measurements in the inner heliosphere". In: *Monthly Notices of the Royal Astronomical Society* 482.2, pp. 1706–1714. DOI: 10.1093/mnras/sty2814.

Stansby, David (2019). "dstansby/pfsspy: pfsspy 0.1.2". In: DOI: 10.5281/ZENODO.2566462.

Stansby, David, Yatharth Rai, Jeffrey Broll, and Siddhant Shaw (2018). "heliopython/heliopy: HelioPy 0.6.3". In: DOI: 10.5281/ZENODO.1697088.

Stone, E.C., A.M. Frandsen, R.A. Mewaldt, E.R. Christian, D. Margolies, J.F. Ormes, and F. Snow (1998). "The Advanced Composition Explorer". In: *Space Science Reviews* 86.1/4, pp. 1–22. ISSN: 00386308. DOI: 10.1023/A:1005082526237.

The Astropy Collaboration et al. (2018). "The Astropy Project: Building an inclusive, open-science project and status of the v2.0 core package". In: *The Astronomical Journal, Volume 156, Issue 3, article id. 123, 19 pp. (2018).* 156. ISSN: 0004-6256. DOI: 10.3847/1538-3881/aabc4f.

Thompson, W. T. (2006). "Coordinate systems for solar image data". In: *Astronomy & Astrophysics* 449.2, pp. 791–803. ISSN: 0004-6361. DOI: 10.1051/0004-6361:20054262.

Titov, Viacheslav S., Zoran Mikić, Tibor Török, Jon A. Linker, and Olga Panasenco (2017). "2010 August 1–2 Sympathetic Eruptions. II. Magnetic Topology of the MHD Background Field". In: *The Astrophysical Journal* 845.2, p. 141. ISSN: 1538-4357. DOI: 10.3847/1538-4357/aa81ce.

Tokumaru, Munetoshi, Daiki Satonaka, Ken'ichi Fujiki, Keiji Hayashi, and Kazuyuki Hakamada (2017). "Relation Between Coronal Hole Areas and Solar Wind Speeds Derived from Interplanetary Scintillation Measurements". In: *Solar Physics* 292.3, p. 41. ISSN: 0038-0938. DOI: 10.1007/s11207-017-1066-7.

Tóth, Gábor (2000). "The ·B=0 Constraint in Shock-Capturing Magnetohydrodynamics Codes". In: *Journal of Computational Physics* 161.2, pp. 605–652. ISSN: 0021-9991. DOI: 10.1006/JCPH.2000.6519.

Tóth, Gábor and Dušan Odstrčil (1996). "Comparison of Some Flux Corrected Transport and Total Variation Diminishing Numerical Schemes for Hydrodynamic and Magnetohydrodynamic Problems". In: *Journal of Computational Physics* 128.1, pp. 82–100. ISSN: 0021-9991. DOI: 10.1006/JCPH.1996.0197.

Ulrich, Roger K and John E Boyden (2006). "CARRINGTON COORDINATES AND SOLAR MAPS". In: *Solar Physics* 235, pp. 17–29. DOI: 10.1007/s11207-006-0041-5.

Verbanac, G., B. Vršnak, A. Veronig, and M. Temmer (2011). "Equatorial coronal holes, solar wind high-speed streams, and their geoeffectiveness". In: *Astronomy & Astrophysics* 526. ISSN: 0004-6361. DOI: 10.1051/0004-6361/201014617.

Wang, Y.-M., Y.-K. Ko, and R. Grappin (2009). "SLOW SOLAR WIND FROM OPEN REGIONS WITH STRONG LOW-CORONAL HEATING". In: *The Astrophysical Journal* 691.1, pp. 760–769. ISSN: 0004-637X. DOI: 10.1088/0004-637X/691/1/760.

Wang, Y.-M and N. R. Sheeley (1990). "SOLAR WIND SPEED AND CORONAL FLUX-TUBE EXPANSION". In: *The Astrophysical Journal* 355, pp. 726–732. URL: http://articles.adsabs.harvard.edu/cgi-bin/nph-iarticle_query?1990ApJ...355..726W&data_type=PDF_HIGH&whole_paper=YES&type=PRINTER&filetype=.pdf.

Webb, David F. and Timothy A. Howard (2012). "Coronal Mass Ejections: Observations". In: *Living Reviews in Solar Physics* 9, p. 3. ISSN: 1614-4961. DOI: 10.12942/lrsp-2012-3.

Winterhalter, D, E J Smith, M E Burton, N Murphy, and D J Mccomas (1994). *The heliospheric plasma sheet*. Tech. rep. A4. DOI: 10.1029/93JA03481.

Yeates, Anthony (2018). "antyeates1983/pfss: First release of pfss code." In: DOI: 10.5281/ZENODO.1472183.

Zeng, Zhicheng, Wenda Cao, and Haisheng Ji (2013). "Observation of magnetic reconnection driven by granular scale advection". In: *Astrophysical Journal Letters* 769.2. ISSN: 20418205. DOI: 10.1088/2041-8205/769/2/L33.

Zeng, Zhicheng, Bin Chen, Haisheng Ji, Philip R Goode, and Wenda Cao (2016). "RESOLVING THE FAN-SPINE RECONNECTION GEOMETRY OF A SMALL-SCALE CHROMOSPHERIC JET EVENT WITH THE NEW SOLAR TELESCOPE". In: *The Astrophysical Journal Letters* 819. DOI: 10.3847/2041-8205/819/1/L3.